J. Fluid Mech. (1992), *vol.* 235, *pp.* 481–510
Printed in Great Britain

Shapes and stability of pendant and sessile dielectric drops in an electric field

By FRED K. WOHLHUTER[1] AND OSMAN A. BASARAN[2]†

[1] Department of Chemical Engineering, University of Tennessee, Knoxville, TN 37996, USA

[2] Chemical Technology Division, Oak Ridge National Laboratory, Oak Ridge, TN 37831-6224, USA

(Received 3 April 1991 and in revised form 24 July 1991)

Axisymmetric equilibrium shapes and stability of linearly polarizable dielectric (ferrofluid) drops of fixed volume which are pendant/sessile on one plate of a parallel-plate capacitor and are subjected to an applied electric (magnetic) field are determined by solving simultaneously the free boundary problem comprised of the Young–Laplace equation for drop shape and the Laplace equation for electric (magnetic) field distribution. When the contact angle that the drop makes with the plate is fixed to be 90° and the distance between the plates is infinite, the results are identical to those of a free drop immersed in a uniform field and resolve discrepancies between previously reported theoretical predictions and experimental measurements. Remarkably, regardless of the value of the ratio of the permittivity (permeability) of the drop to that of the surrounding fluid, κ, drop shapes develop conical tips as drop deformation increases. However, three types of behaviour are found, depending on the value of κ. When $\kappa < \kappa_1$, the drop deformation grows without bound as field strength rises. On the other hand, when $\kappa > \kappa_2 > \kappa_1$, families of equilibrium drop shapes become unstable at turning points with respect to field strength. Beyond the turning points, the unstable families terminate: the mean curvature at the virtually conical drop tip grows without bound. However, in the range $\kappa_1 < \kappa < \kappa_2$, the new results predict that drop deformation exhibits hysteresis, in accord with experiments of Bacri, Salin & Massart (1982) and Bacri & Salin (1982, 1983). Such hysteresis phenomena have been surmized previously on the basis of approximate theories, though they have not been calculated systematically until now. Moreover, detailed computations reveal the importance of varying the drop size and plate spacing, and whether, along the three-phase contact line, the contact line is fixed or the contact angle is prescribed.

1. Introduction

Benjamin Franklin (1751) and later Lord Rayleigh (1879, 1882) pioneered the study of the effects of electric fields and charges on liquid drops. Rayleigh's (1882) pioneering theoretical analysis of the limit of stability of an isolated, surface-charged liquid sphere – an approximation to a real rain drop – inaugurated a century of research on the shapes and stability of electrified drops and electrified interfaces in general, and marked the birth of the science of electrohydrodynamics (Melcher & Taylor 1969). Interest in the effects of electric fields on liquid drops has continued to grow in the last several decades because electrified drops are central to areas of

† Author to whom correspondence should be addressed.

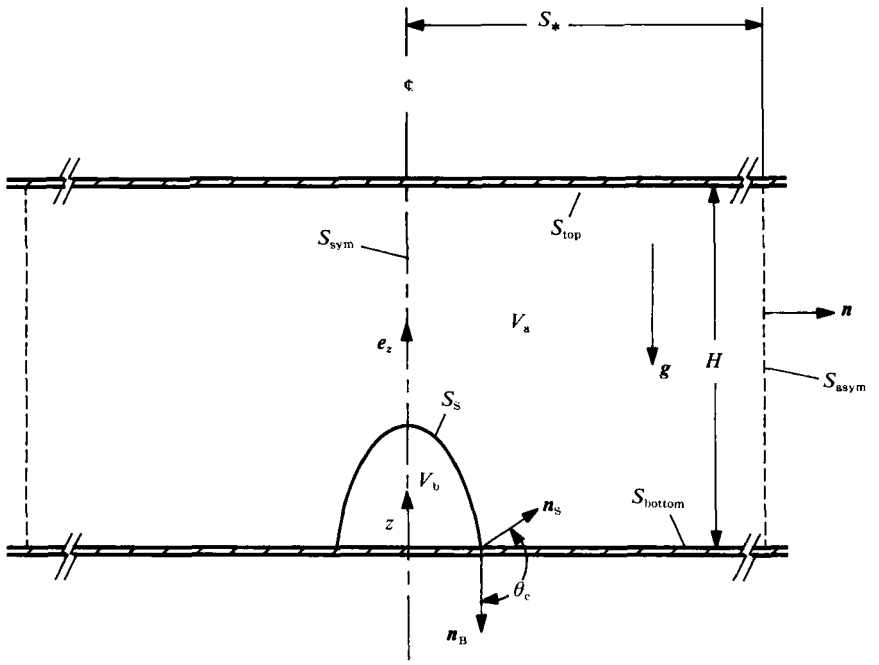

FIGURE 1. Axisymmetric dielectric drop on a face of a circular parallel-plate capacitor.

science and technology as diverse as nuclear physics (Bohr & Wheeler 1939; Cohen, Plasil & Swiatecki 1974; Pelekasis, Tsamopoulos & Manolis 1990), meteorology (Sartor 1969; Beard, Ochs & Kubesh 1989), chemical engineering (Chang & Berg 1985; Basaran, Scott & Byers 1989), and materials processing in reduced gravity (Carruthers & Testardi 1983; Rhim, Chung & Elleman 1989).

The subject of this paper is the axisymmetric equilibrium shapes and stability of linearly polarizable dielectric drops that are surrounded by another linearly polarizable dielectric fluid and are pendant or sessile on a face of a parallel-plate capacitor, as shown in figure 1. It is appropriate to note that the limit in which the ratio of the permittivity of the drop to that of the surrounding fluid κ tends to infinity describes the case of a conducting drop. Also, when the contact angle that the drop makes with the plate is fixed to be 90°, the relative importance of gravitational force is vanishingly small compared to electrical and surface tension forces, and the distance between the plates is infinite, the physics is identical to that of the often-studied problem of a free drop in a uniform external field (cf. Wilson & Taylor 1925; Basaran & Scriven 1989*b*, 1990). Moreover, the equations that govern the response of a drop of a dielectric fluid in an applied electric field are the same as those that govern the response of a drop of a magnetic liquid, or a ferrofluid, in an applied magnetic field (cf. Rosensweig 1979, 1985; Melcher & Taylor 1969; Melcher 1981). Therefore, the results presented here in the context of the electrical problem apply equally well to the magnetic case.

The equilibrium shapes of electrified drops are governed by a nonlinear differential equation, the augmented Young–Laplace equation (see, e.g. Taylor 1964; Miksis 1981, Basaran & Scriven 1982, 1989*a*, *b*, 1990; Adornato & Brown 1983), which is the mathematical statement of the requisite balance on the interface between surface tension, gravitational, and electrical forces. When the fluid inside the drop is a

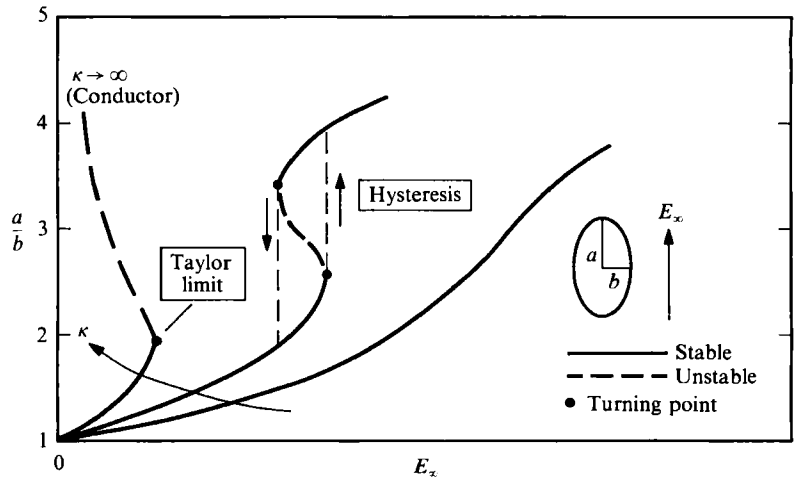

FIGURE 2. Effect of ratio of permittivity of drop to that of surrounding fluid κ on the variation of aspect ratio a/b as a function of dimensionless field strength E_∞.

linearly polarizable dielectric or a perfect conductor and the fluid outside is another linearly polarizable dielectric, the force represented by the electrical pressure term is governed by a linear equation, the Laplace differential equation or an equivalent integral equation for the electrostatic field, but in a region in which part of the boundary, the drop surface, is curved and unknown *a priori*. Thus the potential problem too is nonlinear. Drop shape and electrostatic field need to be found simultaneously. Closed-form or analytical solutions of this free boundary problem are rare; solution by means of numerical methods is a powerful alternative, and the only one except in limiting cases.

In a now celebrated paper, Taylor (1964) approximated the equilibrium shapes of a perfectly conducting ($\kappa \to \infty$), free drop in an external electric field as spheroids. He required the augmented Young–Laplace equation to be satisfied at the north pole and the equator, though not necessarily between. By means of this two-point approximation, Taylor showed that such a drop is neutrally stable with respect to infinitesimal-amplitude perturbations at a turning (or limit) point in applied field strength. The drop shapes in this spheroidal family uncovered by Taylor (1964) are (linearly) stable up to the turning point and are unstable beyond it. The Taylor limit of stability (see figure 2) has now been verified by numerous investigators using various numerical methods. These include the early work of Brazier-Smith (1971) and the more recent and more accurate works of Miksis (1981), who used a boundary-integral (element) method to solve the potential problem, and Basaran & Scriven (1982, 1989*b*, 1990) and Adornato & Brown (1983), who used the Galerkin/finite-element method.

The case of a free dielectric drop, i.e. arbitrary κ, was first analysed by Rosenkilde (1969), who approximated the drop shapes as ellipsoids and used the moment method developed by Chandrasekhar (1969). Rosenkilde found two types of response, depending on whether $\kappa_c < \kappa < \infty$ or $\kappa < \kappa_c$ (where $\kappa_c \approx 20.801$), as shown in figure 2. When $\kappa < \kappa_c$, drop deformation grows without bound as field strength increases, and drop shapes are stable for all values of the applied field strength (and drop deformation). However, when $\kappa > \kappa_c$, drop deformation exhibits hysteresis. In other words, as the electric field strength increases from zero, the drop is stable until a critical field strength. Beyond the first turning point, the unstable branch of the

family of equilibrium drop shapes moves toward lower values of the field strength, and the family subsequently regains stability at a second turning point in field strength. In an experiment, the drop would undergo a finite jump in deformation as the field is increased by an infinitesimal amount at the first turning point and it would undergo a finite reduction in deformation as the field is decreased by an infinitesimal amount at the second turning point. The approximate analyses of Taylor (1964) and Rosenkilde (1969) indicated that the drop deformation would grow indefinitely with increasing (decreasing) field strength.

Miksis (1981), motivated by the desire to predict theoretically the conical tips often seen in experiments, used a boundary-integral method to analyse rigorously the problem of a free dielectric drop in an external electric field. He also generalized Taylor's (1964) two-point method to this problem. With the two-point method, he attained results that were qualitatively the same as those found by Rosenkilde (1969) and determined that $\kappa_c = 18.08$. With his boundary-integral method, Miksis (1981) showed that κ_c lies between 19 and 20 and found the same qualitative response as he and Rosenkilde (1969) did with the spheroidal approximation when $\kappa < \kappa_c$. Moreover, with the more rigorous boundary-integral method, he did not observe hysteresis and found that drop deformation did not grow indefinitely when $\kappa > \kappa_c$. Indeed, he was able to extrapolate that, when $\kappa > \kappa_c$, there is a maximum value of drop deformation at which families of equilibrium shapes terminate.

However, in a series of experiments with aggregates of ferrofluid drops in a magnetic field, Bacri, Salin & Massart (1982) and Bacri & Salin (1982, 1983) reported hysteresis in drop deformation. They also used a spheroidal approximation of the drop shape and energy minimization arguments to model their experiments and thereby surmized that hysteresis can occur when $\kappa > \kappa_c$, where $\kappa_c \geqslant 20$. Their spheroidal approximation predicted that drop deformation can grow indefinitely. In their experiments with aggregates of drops, they estimated a value of κ for their ferrofluid of about 40 for which they observed hysteresis. However, this value of κ was not measured directly, but instead was back-calculated from a fit of the observed hysteresis curve to that obtained by the spheroidal approximation. Nevertheless, these authors recognized the limitation of their spheroidal approximation: the drop shapes they observed became very conical at the tips at large deformations, signalling the breakdown of the spheroidal approximation.

Sherwood (1988), motivated by the experiments of Bacri and co-workers, among other things, analysed theoretically the response of free dielectric drops in an electric field. Instead of determining equilibrium drop shapes directly, Sherwood solved for the time-dependent flow in a dielectric drop induced by an electric field. He assumed conditions of creeping flow to hold both inside and outside the drop and solved the Stokes equations for the flow and the Laplace equation for the electric field distribution by boundary-integral (element) methods. Although he does not state computational times or the number of time-steps required to reach an equilibrium solution, use of a transient simulation to calculate equilibrium shapes can be computationally costly. By means of such transient calculations, Sherwood found hysteresis in drop deformation when $\kappa = 20$. However, he encountered difficulties in following the deformation curves for the shape families shown in figure 2 when $\kappa \geqslant \kappa_c$. At the same value of the field strength, calculated values of the equilibrium aspect ratio differed by over 10% when he followed a drop through the hysteresis loop. Sherwood refined the value of κ_c to be between 19.6 and 19.7. When $\kappa = 25$ and for other values of $\kappa \neq 20$, he was unable to jump from the lower branch of stable solutions to the upper one. He also reported finding equilibrium solutions along the

upper stable branch of solutions if he started his simulations from an initial drop state close to equilibrium, but he could not jump from these states down to ones on the lower branch.

Theoretical and experimental studies of supported – pendant and sessile – magnetic drops reveal results that are qualitatively the same as those for free drops. Berkovsky & Kalikmanov (1985) used a spheroidal approximation to surmize that hysteresis can occur with a magnetic fluid having a high enough susceptibility. Brancher & Zouaoui (1987) also used a spheroidal approximation to surmize that hysteresis can occur and carried out experiments to investigate the formation of conical tips at high field strengths. Berkovsky *et al.* (1987) performed experiments with sessile magnetic drops to investigate primarily the effects of the magnetic properties of the substrate on drop shape and stability. Budnik & Polevikov (1987) determined numerically meniscus shapes and magnetic field distributions in and around sessile drops. However, their computations failed at moderate drop deformations. Moreover, they carried out too few calculations to draw any general conclusions and were unable to detect hysteresis Boudouvis, Puchalla & Scriven (1988) performed carefully controlled experiments and Galerkin/finite-element calculations to probe the effects of wetting, fringing fields, and variable susceptibility on the equilibria and stability of sessile drops of ferrofluid. However, Boudouvis *et al.* did not investigate the possibility of hysteresis in their experiments or calculations.

Accurately calculating equilibrium families of dielectric drops and their stability, and thereby solving the long-standing problem of if and when hysteresis can be observed, are the major goals of this paper. Section 2 presents the equations and boundary conditions that govern the equilibrium shapes of a dielectric drop on a face of a circular parallel-plate capacitor. Section 3 outlines the Galerkin/finite-element formulation of the governing equations for computer-aided calculation of families of drop shapes and their stability. Section 4 presents solution families, drop shapes, and potential and electric fields computed from the theoretical analysis. Finally, in §5 these results are compared to experimental results reported by Bacri *et al.* (1982) and Bacri & Salin (1982, 1983), and opportunities for future research are outlined.

2. Mathematical formulation

2.1. *Governing equations and boundary conditions*

An axisymmetric drop of a linearly polarizable dielectric of permittivity ϵ_b surrounded by another linearly polarizable fluid insulator of permittivity ϵ_a sits on or hangs from, i.e. is sessile on or pendant from, one face of a circular parallel-plate capacitor of radius large compared to distance h between the plates, as shown in figure 1. The surface tension of the drop/ambient fluid interface is σ. One plate of the capacitor is at potential u_0 relative to the other, which is grounded. The drop shape and the electrostatic field $\boldsymbol{E} \equiv -\nabla U$, where U denotes the electrostatic potential inside and outside the drop, are governed by the augmented Young–Laplace and Laplace equations, respectively,

$$-2\mathscr{H} = K - Gz + N_e H^2[E_n^{(a)2} - \kappa E_n^{(b)2} + (\kappa - 1)E_t^2] \quad \text{on} \quad S_S, \tag{1}$$

$$\nabla^2 U = 0 \quad \text{in} \quad V_a \text{ and } V_b. \tag{2}$$

S_S is the drop surface, V_a is the region between the two plates outside the drop, and V_b is the region inside the drop. Equations (1) and (2) are dimensionless because

length is measured in units of R, a characteristic length to be defined shortly, potential U is measured in units of u_0, and

$$\mathscr{H} \equiv R\tilde{\mathscr{H}}, \quad z \equiv \frac{\tilde{z}}{R}, \quad K \equiv \frac{R\Delta p_0}{\sigma}, \quad \boldsymbol{E} \equiv \frac{R\tilde{\boldsymbol{E}}}{u_0}, \tag{3}$$

$$H \equiv \frac{h}{R}, \quad \kappa \equiv \frac{\epsilon_b}{\epsilon_a}, \quad N_e \equiv \frac{\epsilon_a R u_0^2}{2\sigma h^2}, \quad G \equiv \frac{gR^2\Delta\rho}{\sigma}. \tag{4}$$

A variable appearing with a tilde above it is dimensional; without a tilde it is dimensionless. $2\mathscr{H}$ is twice the local mean curvature of the interface and is the negative of the surface divergence of the field of unit normals to the drop surface, i.e. $2\mathscr{H} = -\nabla_S \cdot \mathbf{n}_S$; z is distance measured from the origin in the direction opposite to gravity; reference pressure K is simply the pressure excess Δp_0 at the level of the plane called $z = 0$ in the drop, measured in units of half the capillary pressure within an uncharged spherical drop of radius R. E_n and E_t are the normal and tangential components, respectively, of the electric field at the drop surface. Subscripts and superscripts a and b denote the exterior and interior of the drop, respectively. κ is the ratio of the permittivity, or the dielectric constant, of the drop material to that of the surrounding fluid. N_e is the electric bond number and its square root, $N_e^{\frac{1}{2}} = (u_0/h)(\epsilon_a R/2\sigma)^{\frac{1}{2}}$, is the dimensionless parallel-plate electric field strength. It is supposed hereafter that the effect of gravity is far less than that of surface tension, i.e. the gravitational bond number $G \to 0$ is vanishingly small; g is the acceleration due to gravity and $\Delta\rho$ the density difference between the drop and surrounding fluid. Though values of $\Delta\rho \gg 0$ correspond to drops and $\Delta\rho \ll 0$ to bubbles, they need not be distinguished here because $G \to 0$. When $G \to 0$, K is simply the dimensionless excess pressure in the drop over ambient pressure. The reference pressure K is set by constraining the drop volume to be a fixed amount V_0:

$$V = V_0. \tag{5}$$

The governing equations (1) and (2) are solved subject to the boundary conditions

$$\boldsymbol{n}_S \times \boldsymbol{e}_z = \mathbf{0} \quad \text{at} \quad z = a \text{ along } S_{sym}, \tag{6}$$

$$\delta\theta_c = \delta[\cos^{-1}(\boldsymbol{n}_S \cdot \boldsymbol{n}_B)] = 0 \quad \text{or} \quad \delta\boldsymbol{x}_S = \mathbf{0} \quad \text{at} \quad z = 0, \tag{7a, b}$$

$$U = 1 \quad \text{on} \quad S_{bottom}, \quad U = 0 \quad \text{on} \quad S_{top}, \tag{8, 9}$$

$$\boldsymbol{n} \cdot \nabla U = 0 \quad \text{on} \quad S_{sym} \text{ and } S_{asym}, \tag{10}$$

$$E_t^{(a)} = E_t^{(b)} \quad \text{or} \quad U^{(a)} = U^{(b)}, \quad E_n^{(a)} = \kappa E_n^{(b)} \quad \text{on} \quad S_S, \tag{11, 12}$$

where $\boldsymbol{e}_z$ is a unit vector and a is the length of the drop in the z-direction. Equation (6) is the condition that the drop profile be axially symmetric. Equation (7) is the boundary condition at the contact line (circle), where $\boldsymbol{x}_S \in S_S$, θ_c is the contact angle and $\boldsymbol{n}_B$ is the unit normal to the bottom plate. Equation (7a) is the limiting case in which the contact angle finally attains its equilibrium value on a smooth, homogeneous solid – the fixed contact angle condition – and (7b) is the opposite limit of a virtually fixed contact circle, which is not uncommonly seen on shorter timescales or if there is a hole with a sharp edge at which the contact circle behaves as though pinned – the fixed contact line condition. Equations (8) and (9) are the boundary conditions that the surface potentials of the two plates must be uniform because they are conducting. Of course, interchanging the potentials of the two plates has no effect on drop shape and stability. Equation (10) is the condition that the electrostatic field and potential be axially symmetric and that far from the drop

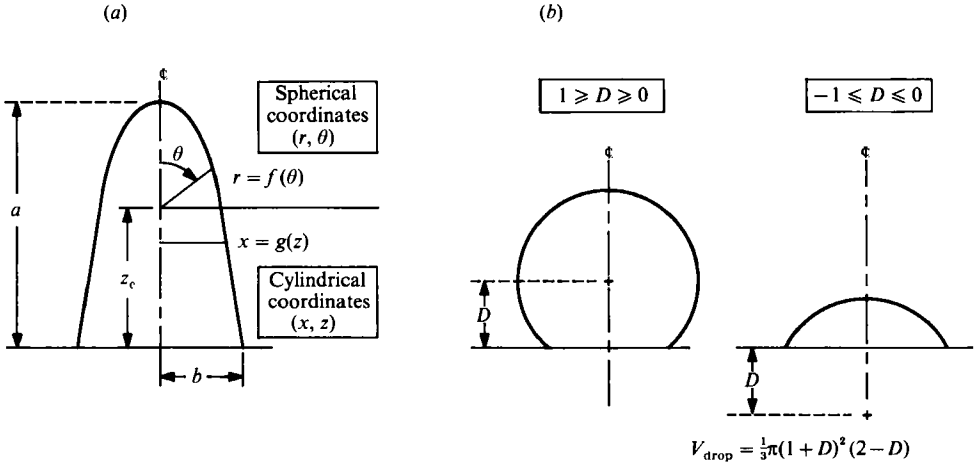

FIGURE 3. Equilibrium drop shape: (*a*) drop shape represented in a composite coordinate system of cylindrical and spherical coordinates; (*b*) drop shapes are sections or segments of spheres when $N_e \to 0$ and $G \to 0$.

the field asymptotically approach a vertically directed uniform field which has strength $1/H$. Equations (11) and (12) are the conditions that the tangential component of the electric field and the normal component of the electric displacement be continuous across the interface (see e.g. Landau & Lifshitz 1960).

2.2. *Equilibrium drop shape in the absence of external forces*

When gravitational and electrical forces are vanishingly small compared to surface tension forces, the equilibrium drop shapes are segments of spheres and are conveniently parametrized in terms of the single parameter d, the signed distance from the centre of the sphere to the plate, or its ratio to the radius of the sphere, i.e. $D \equiv d/R$. If the drop shape is represented in cylindrical coordinates (x, z) near the supporting plate and in spherical coordinates (r, θ) near the tip, then the interface shape function is

$$x = g(z) = (1-(D-z)^2)^{\frac{1}{2}}, \quad 0 \leqslant z \leqslant z_c \tag{13}$$

near the plate and

$$r = f(\theta) = -(z_c - D)\cos\theta + (1-(z_c-D)^2\sin^2\theta)^{\frac{1}{2}}, \quad z \geqslant z_c, \quad 0 \leqslant \theta \leqslant \tfrac{1}{2}\pi \tag{14}$$

everywhere else, as shown in figure 3. z_c is the length of the portion of the major axis of the drop that is represented in cylindrical coordinates and is defined in the next section. The drop volume is

$$V_0 = \tfrac{1}{3}\pi(1+D)^2(2-D). \tag{15}$$

When $D = 0$ the drop is a hemisphere; when $D = 1$ the sphere touches the top or bottom plate at one point; and when $D = -1$ there is no sphere. If the contact angle that the drop makes with the supporting plate is fixed, then the contact angle $\theta_c = \cos^{-1} D$.

3. Galerkin/finite-element analysis

Because of the highly deformed drop shapes that are seen in experiments and, therefore, must be calculated, a composite coordinate system made of a region of cylindrical coordinates and one of spherical coordinates is used in this paper (see

figure 3(*a*). The use of such composite coordinate domains in free boundary problems was pioneered by Saito & Scriven (1981) in their study of slot coating and has been successfully applied by Ungar & Brown (1985) to solidification problems, Gupte & Tsamopoulos (1989) to the study of chemical vapour infiltration, and Benner, Basaran & Scriven (1991) to the study of rotating drop breakup. The transition between the two regions is chosen such that a constant fraction w_c of the major axis of the drop a is represented in cylindrical coordinates, $z_c = w_c a$. The problem domains in the cylindrical coordinate region are $V_b \equiv \{(x,z): 0 \leqslant x \leqslant g(z), 0 \leqslant z \leqslant z_c\}$ inside the drop, and $V_a \equiv \{(x,z): g(z) \leqslant x \leqslant S_*, 0 \leqslant z \leqslant z_c\}$ outside the drop, where S_* is the domain length measured along the plate. These regions are tessellated into a set of $N_z \times N_{rb}$ and $N_z \times N_{ra}$ quadrilateral elements inside and outside the drop, respectively, where N_z is the number of elements in the z-direction and N_{rb} and N_{ra} are the number of elements in the x-direction inside and outside the drop, respectively. The origin of the spherical coordinate system is located on the axis of symmetry at $z = z_c$. Then the problem domains in the spherical coordinate region are $V_b \equiv \{(r,\theta): 0 \leqslant r \leqslant f(\theta), 0 \leqslant \theta \leqslant \frac{1}{2}\pi\}$ inside the drop and $V_a \equiv \{(r,\theta): f(\theta) \leqslant r \leqslant r_*(\theta), 0 \leqslant \theta \leqslant \frac{1}{2}\pi\}$ outside the drop. Here $r_*(\theta) = H'/\cos\theta$ for $0 \leqslant \theta \leqslant \theta_c$ and $r_*(\theta) = S_*/\sin\theta$ for $\theta_c \leqslant \theta \leqslant \frac{1}{2}\pi$, where $H' = H - z_c$, and $\theta_c = \tan^{-1}(S_*/H')$. These regions are tessellated into a set of $N_\theta \times N_{rb}$ and $N_\theta \times N_{ra}$ quadrilateral elements, where N_θ is the number of elements in the θ-direction and N_{rb} and N_{ra} are the number of elements in the r-direction inside and outside the drop, respectively. A sample mesh or tessellation with a very coarse grid (not used in the calculations) is shown in figure 4(*a*, *b*).

The vertices, midpoints of sides, and midpoints of the elements are called nodes. The elements are bordered by the fixed spines (Kistler & Scriven 1983) z_{2i-1} and θ_{2j-1}:

$$z_{2i-1} = s_{2i-1} z_c, \quad i = 1, \ldots, N_z + 1, \quad \text{for} \quad 0 \leqslant z \leqslant z_c \tag{16a}$$

in the cylindrical coordinate system, and

$$\theta_{2j-1} = t_{2j-1} \theta_c, \quad j = 1, \ldots, N_c + 1 \quad \text{for} \quad 0 \leqslant \theta \leqslant \theta_c, \tag{16b}$$

$$\theta_{2j-1} = t_{2j-1}(\tfrac{1}{2}\pi - \theta_c) + \theta_c, \quad j = N_c + 2, \ldots, N_\theta + 1 \quad \text{for} \quad \theta_c < \theta \leqslant \tfrac{1}{2}\pi \tag{16c}$$

in the spherical coordinate system. Here N_c is the number of elements in the θ-direction for $0 \leqslant \theta \leqslant \theta_c$. In the part of the domain represented in cylindrical coordinates, the elements are also bordered by the curves

$$x_{2k-1}(z) = g(z)\, v_{2k-1}, \quad k = 1, \ldots, N_{rb} + 1 \tag{17a}$$

inside the drop, and

$$x_{2l-1}(z) = g(z) + [S_* - g(z)]\, w_{2l-1}, \quad l = 1, \ldots, N_{ra} + 1 \tag{17b}$$

outside the drop. In the portion of the domain represented in spherical coordinates, the elements are bordered by the curves

$$r_{2k-1}(\theta) = f(\theta)\, v_{2k-1}, \quad k = 1, \ldots, N_{rb} + 1 \tag{17c}$$

inside the drop, and

$$r_{2l-1}(\theta) = f(\theta) + [r_*(\theta) - f(\theta)]\, w_{2l-1}, \quad l = 1, \ldots, N_{ra} + 1 \tag{17d}$$

outside the drop. These curves move proportionally to the free surface along the spines. In (17*a–d*), s_{2i-1}, t_{2j-1}, v_{2k-1}, and w_{2l-1} are weights chosen to concentrate the elements near the drop surface and drop tip, where they are needed. Equations (16)

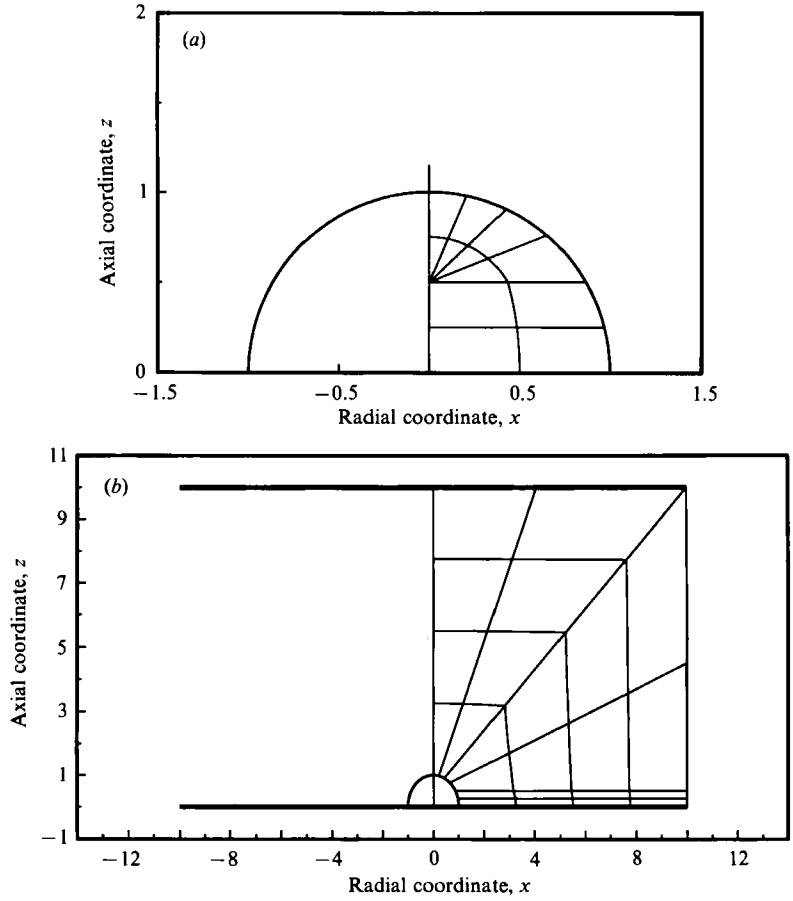

FIGURE 4. Finite-element mesh (*a*) inside the drop and (*b*) outside the drop. This coarse mesh is for illustrative purposes and was not used in calculations. Here $N_z = 2$, $N_\theta = 4$, $N_{rb} = 2$, and $N_{ra} = 4$.

and (17) prescribe the positions of only the vertex-nodes of the elements. Mid-side and mid-element nodes are located by requiring mid-elements spines to satisfy $z_{2i} = \frac{1}{2}(z_{2i-1} + z_{2i+1})$, $i = 1, \ldots, N_z$, $\theta_{2j} = \frac{1}{2}(\theta_{2j-1} + \theta_{2j+1})$, $j = 1, \ldots, N_\theta$, and by requiring the weights to satisfy $v_{2k} = \frac{1}{2}(v_{2k-1} + v_{2k+1})$, $k = 1, \ldots, N_{rb}$, and $w_{2l} = \frac{1}{2}(w_{2l-1} + w_{2l+1})$, $l = 1, \ldots, N_{ra}$, which are enough to ensure that the Jacobian determinant of the isoparametric mapping introduced below does not vanish.

Each curvilinear element is mapped onto the unit square with coordinates (ξ, η), $0 \leqslant \xi, \eta \leqslant 1$ by the isoparametric transformation (Strang & Fix 1973). On the unit square, nine biquadratic basis functions are defined in the standard way (Strang & Fix 1973). The basis functions have global numbers $i \in \{1, 2, \ldots, I\}$, where $I = (2N_\theta + 2N_z + 1)(2N_{ra} + 2N_{rb} + 1)$.

The unknown electrostatic potential is expanded in a set of biquadratic basis functions ψ^i *as*

$$U(\boldsymbol{x}) = \sum_{i=1}^{I} \alpha_i \psi^i(\xi, \eta), \tag{18}$$

where $\boldsymbol{x} \in V_a$ or V_b. The coefficients α_i are values of the potential at the nodes and $\boldsymbol{\alpha} = (\alpha_1, \ldots, \alpha_I)$ is the vector of all of them.

At the drop surface, only the basis functions ψ^s associated with free-surface nodes are non-zero. The free surface is interpolated globally as

$$\begin{pmatrix} g(z) \\ f(\theta) \end{pmatrix} = \sum_{s=1}^{S} \beta_s \psi^s(\xi, \eta = 0). \tag{19}$$

The drop surface maps onto the $\eta = 0$ edge of the (ξ,-η)-domain. The coefficients β_s are nodal values of free surface location, $\boldsymbol{\beta} = (\beta_1, \ldots, \beta_S)$ is the vector of all of them, and $S = 2N_\theta + 2N_z + 1$ is the total number of free-surface nodes.

The Galerkin weighted residuals of the Young–Laplace equation are

$$\begin{aligned} R_s^{\mathrm{YL}} &= \int_{S_S} \{2\mathscr{H} + K + N_e H^2 (E_n^{(a)2} - \kappa E_n^{(b)2} + (\kappa - 1) E_t^2)\} \psi^s \boldsymbol{e}_k \cdot \boldsymbol{n}_S \, \mathrm{d}S \\ &= 0, \quad s = 1, \ldots, S, \end{aligned} \tag{20}$$

where $\boldsymbol{e}_k = \boldsymbol{e}_x$ over the portion of the drop surface represented in cylindrical coordinates and $\boldsymbol{e}_k = \boldsymbol{e}_r$ over that represented in spherical coordinates. The curvature term in (20) is integrated by parts using the surface divergence theorem (Weatherburn 1927)

$$\int_S 2\mathscr{H} \psi^s \boldsymbol{e}_k \cdot \boldsymbol{n} \, \mathrm{d}S = \oint_L \psi^s \boldsymbol{e}_k \cdot \boldsymbol{m} \mathrm{d}L - \int_S \nabla_S \cdot (\psi^s \boldsymbol{e}_k) \, \mathrm{d}S, \tag{21}$$

where $\boldsymbol{m}$ is a unit vector tangent to the surface S and normal to the curve L bounding S, to reduce terms involving the drop shape to first order in g and f (Basaran & Scriven 1990):

$$\begin{aligned} R_s^{\mathrm{YL}} = \int_0^{z_c} \Bigg\{ & - \frac{(1+g_z^2)^{\frac{1}{2}} \psi^s + g g_z \psi_z^s}{(1+g_z^2)^{\frac{1}{2}}} \\ & + [K + N_e H^2 (E_n^{(a)2} - \kappa E_n^{(b)2} + (\kappa - 1) E_t^2)] g \psi^s \Bigg\} \mathrm{d}z \\ + \int_0^{\frac{1}{2}\pi} \Bigg\{ & - \frac{f f_\theta \psi_\theta^s + \psi^s (2f^2 + f_\theta^2)}{(f^2 + f_\theta^2)^{\frac{1}{2}}} \\ & + [K + N_e H^2 (E_n^{(a)2} - \kappa E_n^{(b)2} + (\kappa - 1) E_t^2)] f^2 \psi^s \Bigg\} \sin\theta \, \mathrm{d}\theta = 0. \end{aligned} \tag{22}$$

The Galerkin-weighted residuals of the Laplace equation associated with nodes inside the drop are

$$R_i^{\mathrm{L}} = \int_{V_b} \psi^i \nabla^2 U \, \mathrm{d}V = 0, \quad i = 1, \ldots, (2N_\theta + 2N_z + 1)(2N_{rb} + 1), \tag{23}$$

and those associated with nodes outside the drop are

$$R_i^{\mathrm{L}} = \int_{V_a} \psi^i \nabla^2 U \, \mathrm{d}V = 0, \quad i = 1, \ldots, (2N_\theta + 2N_z + 1)(2N_{ra} + 1). \tag{24}$$

The Laplace residuals are also reduced to first-order in U by means of the divergence theorem. The electrostatic potential is continuous across the drop surface (see (11)). Therefore, for those nodes lying along the drop surface, the versions of (23) and (24)

that result following the integration by parts are summed and the result simplified by means of (12):

$$R_i^{\mathrm{L}} = \int_{V_a} \nabla\psi^i \cdot \nabla U^{(a)}\,\mathrm{d}V + \kappa \int_{V_b} \nabla\psi^i \cdot \nabla U^{(b)}\mathrm{d}V = 0, \quad i = 1, \ldots, I. \tag{25}$$

Weighted by each ψ^s in turn (22) provides S augmented Young–Laplace residual equations $(R_1^{\mathrm{YL}}, \ldots, R_S^{\mathrm{YL}}) \equiv \boldsymbol{R}^{\mathrm{YL}}$, the same number as there are free-surface coefficients in (19). Similarly, weighted by each ψ^i in turn (25) provides I Laplace residual equations $(R_1^{\mathrm{L}}, \ldots, R_I^{\mathrm{L}}) \equiv \boldsymbol{R}^{\mathrm{L}}$, the same number as there are electrostatic potential coefficients in (18).

The volume constraint (4) is rewritten as the $\mathscr{N}+1-st$ residual, where $\mathscr{N} = S+I$,

$$R_{\mathscr{N}+1} \equiv R^{\mathrm{VC}} = V - V_0 = 0. \tag{26}$$

In anticipation of turning points, another residual is defined which specifies an adaptive choice of parameter $\mathscr{P}$ (Abbott 1978),

$$R_{\mathscr{N}+2} \equiv \mathscr{P} - \mathscr{P}_0 - \Delta\mathscr{P} = 0, \tag{27}$$

where $\mathscr{P}_0$ is the value of the parameter at a known solution $\boldsymbol{\omega}^*$ on a family of solutions and the parameter step size $\Delta\mathscr{P}$ is a specified increment to a new solution of $\boldsymbol{R}(\boldsymbol{\omega}) \equiv (\boldsymbol{R}^{\mathrm{YL}}, \boldsymbol{R}^{\mathrm{L}}, R^{\mathrm{VC}}, R_{\mathscr{N}+2}) = \boldsymbol{0}$ on the same family. The method for choosing the parameter $\mathscr{P}$ from among the entries of the solution $\boldsymbol{\omega} \equiv (\boldsymbol{\beta}, \boldsymbol{\alpha}, K, N_e)$ is described by Abbott (1978). Here, it was found adequate to restrict the choice of $\mathscr{P}$ to the subset $(\boldsymbol{\beta}, K, N_e)$.

The nonlinear set of algebraic equations $\boldsymbol{R}(\boldsymbol{\omega}) = \boldsymbol{0}$ is solved simultaneously by Newton's method (Ortega & Rheinboldt 1970): given an initial approximation $\boldsymbol{\omega}^{(0)}$ to the solution, the $(k+1)$th approximation is obtained from the kth by

$$\boldsymbol{J}(\boldsymbol{\omega}^{(k)})\,(\boldsymbol{\omega}^{(k+1)} - \boldsymbol{\omega}^{(k)}) = -\boldsymbol{R}(\boldsymbol{\omega}^{(k)}), \tag{28}$$

where $\boldsymbol{J} \equiv \partial\boldsymbol{R}/\partial\boldsymbol{\omega}$ is the Jacobian matrix of partial derivatives. The linear system that results at each Newton iteration is then solved by direct factorization with a modification (Walters 1980) of Hood's (1976) frontal solver. The Newton iteration was continued until the Euclidean norm (Isaacson & Keller 1966), i.e. the square root of the sum of squares, of both solution update $\Delta\boldsymbol{\omega}^{(k+1)}$ and residuals $\boldsymbol{R}^{(k)}$ were less than a prescribed tolerance Δe. In this paper $\Delta e = 10^{-6}$. The theoretical asymptotic convergence of Newton iteration is second order (Isaacson & Keller 1966). That quadratic convergence is attained is an important test of the correct formulation of the Jacobian and, if the residuals are also right, error-free coding of the computation. Establishing the insensitivity, i.e. robustness, of computed solutions to refinement of the discretization or tessellation is also crucial and is discussed below.

Critical to Newton's method is the initial estimate $\boldsymbol{\omega}^{(0)}$, which must be accurate enough to fall within the domain of convergence of the method. Tracking of solution families begins in the next section with the following initial estimate: the initial drop shape, $g^{(0)}(z)$ and $f^{(0)}(\theta)$, is given by (13) and (14),

$$U^{(0)} = \begin{cases} 0 & \text{everywhere in } V_a \text{ except on } S_{\mathrm{bottom}}, \\ 1 & \text{everywhere in } V_b \text{ and on } S_{\mathrm{bottom}} \text{ and } S_S \end{cases} \tag{29}$$

$$K^{(0)} = 2, \quad N_e^{(0)} = 0. \tag{30, 31}$$

Thereafter a converged solution $\boldsymbol{\omega}^*(\mathscr{P}_0)$ is available; the initial estimate for solution

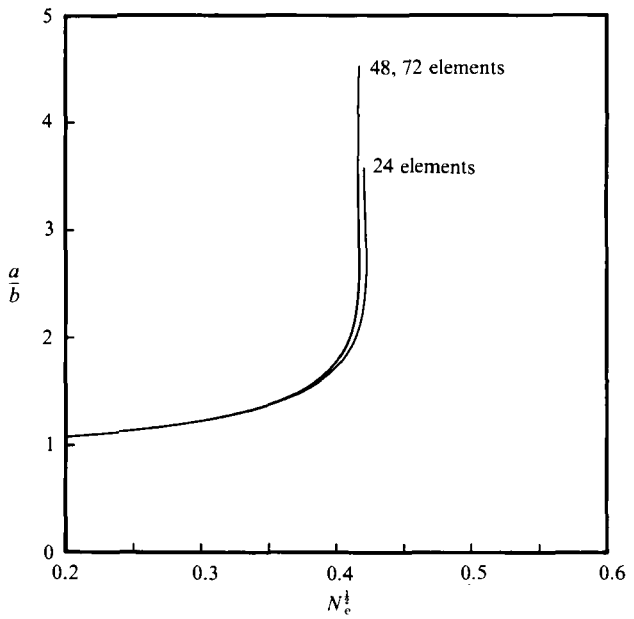

FIGURE 5. Sensitivity of variation of aspect ratio a/b with field strength to mesh refinement in the r-direction outside the drop.

at parameter value $\mathscr{P} = \mathscr{P}_0 + \Delta\mathscr{P}$ is obtained by zeroth-order continuation over the increment $\Delta\mathscr{P}$. Increments in $\Delta\mathscr{P}$ were chosen here so that Newton's method typically converged in four to six iterations.

While tracking solution families to be reported in the next section, no bifurcation points but many turning points were encountered. Because turning points signal stability limits (see e.g. Iooss & Joseph 1990; Ungar & Brown 1982), they are often more important than solutions themselves.

The algorithm was programmed in FORTRAN. Program development and preliminary calculations were done on a DECstation 3100 at the Oak Ridge National Laboratory. All the calculations reported in this paper were carried out on a CRAY-YMP at the Florida State University Computing Center.

The domain was tessellated into $N_z = 6$, 8, and 10 non-uniform elements in the z-direction and $N_\theta = 8$, 12 and 16 uniform elements in the θ-direction along the drop surface and $N_{r\mathrm{b}} = 6$, 8, and 10 non-uniform elements inside the drop and $N_{r\mathrm{a}} = 24$, 48, and 72 non-uniform elements outside the drop in the other direction, i.e. in the r-direction in spherical coordinates and in the x-direction in cylindrical coordinates. Calculations were made to show the sensitivity of the variation of aspect ratio a/b with field strength to refinement in tessellation for a drop with $\kappa = 21$ and making a fixed contact angle of 90° with the supporting plate. The maximum difference in the calculated aspect ratio remains less than 0.1% as the mesh is refined in the z- and θ-directions and in the r-direction inside the drop. In figure 5, the maximum difference in the curves is about 1% when the number of r-elements outside the drop is increased from 24 to 48. However, despite this *apparently* small difference in the curves, there are major qualitative differences in the results obtained with these two meshes, which will be described in the next section. When the number of r-elements outside the drop is increased from 48 to 72, the maximum difference between the curves is less than 0.1%. Therefore, the results reported in the next section were

obtained on a tessellation of $N_z = 8$, $N_\theta = 12$, $N_{r_b} = 8$, and $N_{r_a} = 48$, a total of 1120 elements and 4676 unknowns, unless stated otherwise. The calculation time for one parameter step was approximately 30 CPU seconds with this mesh. Typically 100–200 parameter steps were required to fully understand the response of a drop in a situation in which κ, D, and the contact-line boundary condition were specified.

4. Results

Figure 6 (*a*, *b*) shows how the aspect ratio of dielectric drops making a fixed contact angle of 90° ($D = 0$) with the supporting plate varies with parallel-plate field strength $N_e^{\frac{1}{2}}$. There are three types of response. (i) When $\kappa < 20.25 \pm 0.25$ the drops are everywhere stable over the region of field strengths examined and drop deformation increases monotonically with increasing field strength. (ii) When $21.75 \pm 0.25 \geqslant \kappa \geqslant 20.25 \pm 0.25$ the drop deformation exhibits hysteresis. Drop shapes are stable along the branch up to the first turning point and unstable along the branch between the two turning points. Beyond the second turning point, the drop regains stability and its deformation increases with increasing field strength over the region of field strengths examined. (iii) When $\kappa > 21.75 \pm 0.25$, families of equilibrium drop shapes become unstable at a turning point with respect to field strength. Beyond the turning points, the unstable families terminate: this is a fact to which we return below. The curve for $\kappa \to \infty$ is the limiting case of a conducting drop. The stability limit of such a conducting drop determined here agrees well with those reported by Taylor (1964), Miksis (1981), Adornato & Brown (1983), and Basaran & Scriven (1982, 1989*b*, 1990).

Table 1 shows that finite-element prediction of the transition from shape families displaying monotonic increase of a/b with $N_e^{\frac{1}{2}}$ to shape families turning back to lower values of the field strength at a turning point agrees well with previously published results. Figure 6 also makes clear why Sherwood (1988) was unsuccessful in jumping from the lower branch of stable solutions to an upper branch of stable solutions at $\kappa = 25$.

The expression for twice the local mean curvature, $2\mathscr{H}$, involves second derivatives of the interface shape functions, f and g. It is illegal, in the finite-element sense (Strang & Fix 1973), to calculate second derivatives with the class of admissible C^0 basis functions used in this paper. Therefore, an average mean curvature at the drop tip is calculated here by means of the surface divergence theorem, (21), with $\psi^s = 1$, over the first finite element $0 \leqslant \theta \leqslant \theta_1 \ll 1$:

$$\langle 2\mathscr{H} \rangle = \frac{\displaystyle\int_{\text{Element 1}} 2\mathscr{H} \boldsymbol{e}_r \cdot \boldsymbol{n} \, \mathrm{d}S}{\displaystyle\int_{\text{Element 1}} \boldsymbol{e}_r \cdot \boldsymbol{n} \, \mathrm{d}S} = \frac{\displaystyle -\int_{\text{Element 1}} \nabla_s \cdot \boldsymbol{e}_r \, \mathrm{d}S + f \sin\theta \boldsymbol{e}_r \cdot \boldsymbol{m}|_{\theta=\theta_1}}{\displaystyle\int_{\text{Element 1}} \boldsymbol{e}_r \cdot \boldsymbol{n} \, \mathrm{d}S}. \tag{32}$$

Figure 7 shows the variation of the reciprocal of the average mean curvature at the drop tip with increasing aspect ratio for initially hemispherical ($D = 0$) drops whose contact angles are prescribed. Plainly, the mean curvature at the drop tip increases as drop deformation increases. When $\kappa > 21.75 \pm 0.25$, the mean curvature at the drop tip initially increases slowly, and then rapidly goes to infinity. Evidently, these families terminate when drop aspect ratio reaches some finite value. This finding agrees with the boundary-element prediction of Miksis (1981) and points to the dangers of using such *ad hoc* approaches as the spheroidal approximation, which incorrectly predicts that equilibrium solutions exist for all values of the drop aspect

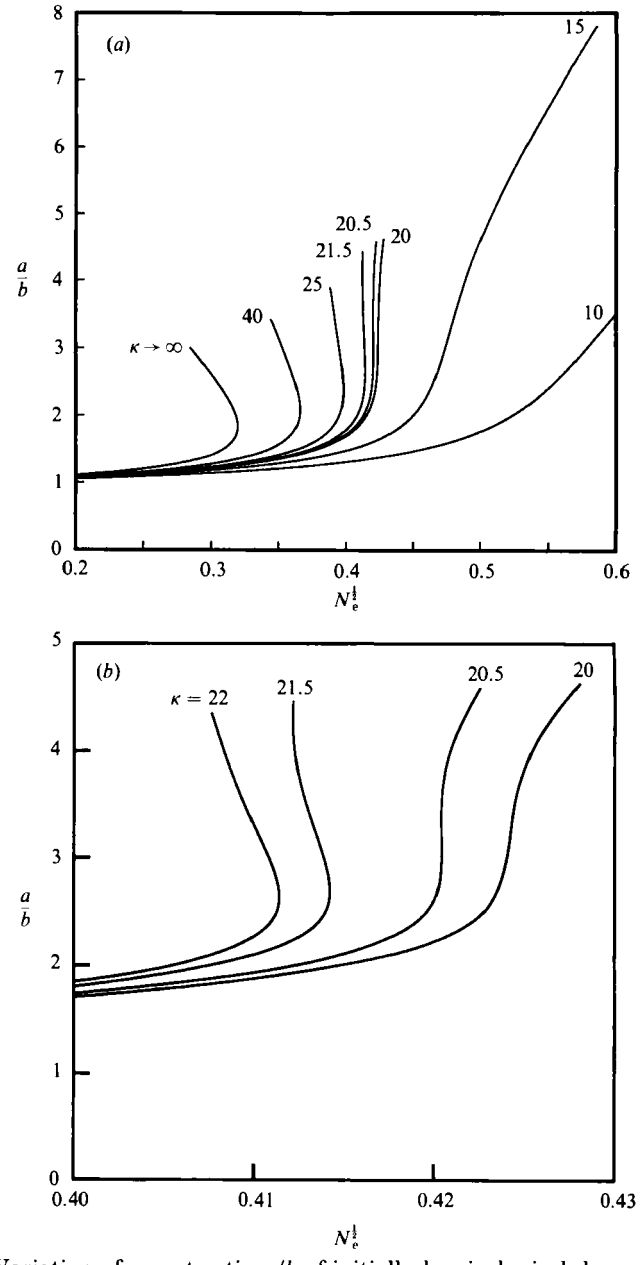

FIGURE 6. (*a*) Variation of aspect ratio a/b of initially hemispherical drops whose contact angles are prescribed with field strength for various values of κ. (*b*) Blow-up of the region showing transition in types of response.

ratio. When $\kappa > 21.75 \pm 0.25$, the computations end with the last calculated point shown in figure 7. To carry the calculations to a point where the mean curvature at the drop tip is virtually infinite would require finite-element tessellations with an order of magnitude or more as many unknowns as those used in this paper. Miksis (1981) too was forced to stop his computations before he could reach the point of termination of a shape family. When $\kappa < 21.75 \pm 0.25$, the mean curvature at the

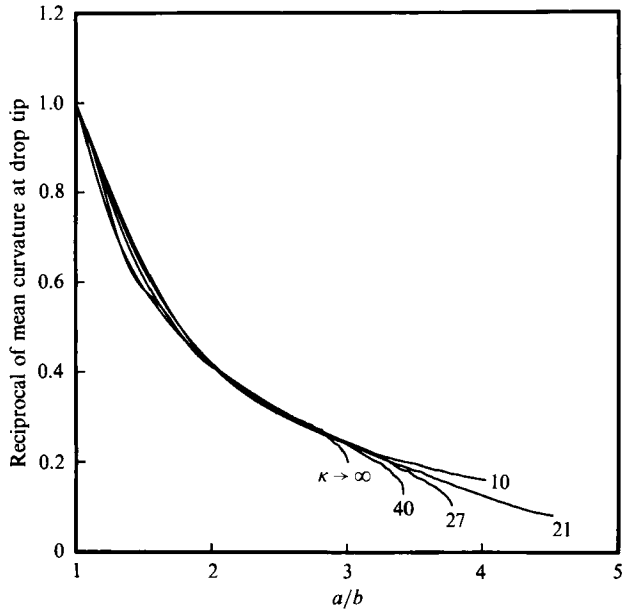

FIGURE 7. Variation of the reciprocal of the average mean curvature at the drop tip with increasing ratio for initially hemispherical drops whose contact angles are prescribed.

Reference	Method of solution	κ_c
Rosenkilde (1969)	Ellipsoidal approximation with moment method	20.8
Miksis (1981)	Spheroidal approximation with two-point method	18.1
	Boundary-integral method	19–20
Sherwood (1988)	Transient analysis/ boundary-integral method	19.6–19.7
This work	Finite-element method	20–20.5

TABLE 1. Critical value of the ratio of the drop permittivity to that of the surrounding fluid, κ_c, for transition from monotonic increase of drop deformation along a shape family to shape families turning back to lower values of the field strength

drop tip decreases smoothly with drop deformation and tends to infinity only asymptotically. When $21.75 \pm 0.25 < \kappa < 20.25 \pm 0.25$, it was heretofore not known that the mean curvature at the drop tip tends to infinity only as the aspect ratio goes to infinity and, consequently, that these families exhibiting hysteresis exist for all values of drop deformation.

Using 24 quadratic elements (instead of 48) in the r-direction outside the drop, while keeping the number of elements unchanged elsewhere, the lower limit of κ giving rise to hysteresis is reduced to a value between 19 and 20 and the upper limit is increased to a value between 25 and 30. When the mesh in the r-direction outside the drop is refined from 24 to 48 quadratic elements, the value of the electric field strength at the first turning point for $\kappa = 25$ changes by less than 1.5 %. Furthermore, when $\kappa = 25$ the family of drop shapes computed with a tessellation of 24 elements in the r-direction outside the drop incorrectly exhibits hysteresis, whereas that computed with a tessellation of 48 elements in the r-direction outside the drop does

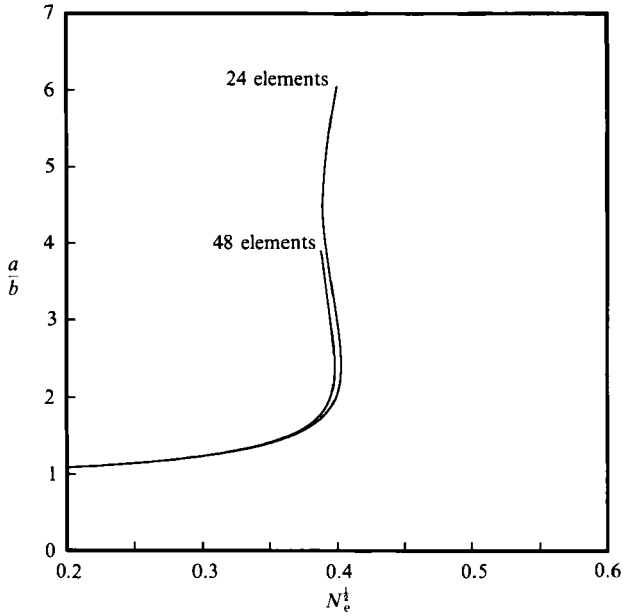

FIGURE 8. Variation in the calculated response of initially hemispherical drops whose contact angles are prescribed with mesh refinement in the r-direction outside the drop when $\kappa = 25$.

not, as shown in figure 8. Results of mesh refinement studies show that qualitative changes (i.e. hysteresis versus no hysteresis) in solution behaviour are the consequence when too few elements are deployed in the tessellation. Moreover, we have shown that close agreement up to the first turning point between shape families calculated with different meshes is not necessarily a sure indication that the calculated results are mesh-independent. The mesh-independence or robustness of the computed solutions must be demonstrated over the whole range of parameters (cf. figures 5 and 8). Miksis (1981) provides a one point comparison of results he obtained using three tessellations which agree to within better than 0.5%. However, his example is of a drop which is everywhere stable, $\kappa = 10$, rather than of one which exhibits hysteresis and is thus extremely sensitive to mesh refinement. Sherwood (1988) reports results of mesh refinement when $\kappa = 20$. In this situation, the aspect ratio of the drop after it has jumped from the lower branch of the hysteresis curve to the upper branch differs by 5% for the different meshes that he used. However, the difference between the solutions that he obtained using different meshes falls to about 1% as he follows the upper branch of the hysteresis curve. This is to be expected and is a drawback of the transient approach that he used relative to the method of solution employed here and by Miksis (1981). With a transient algorithm, a simulation should be started from an initial state as close as possible to the desired final steady or equilibrium state, for otherwise time truncation error accumulates and destroys the accuracy of the calculated solutions at large times.

Figure 9 shows how aspect ratio varies with field strength for the case of initially hemispherical drops ($D = 0$) whose contact lines are fixed. The same three types of response are exhibited by drops whose contact lines are fixed as ones whose contact angles are prescribed. (i) When $\kappa < 14.5 \pm 0.5$, the drops are everywhere stable over the region of field strengths examined and the drop deformation increases monotonically with increasing field strength. (ii) When $20.5 \pm 0.5 \geqslant \kappa \geqslant 14.5 \pm 0.5$ the

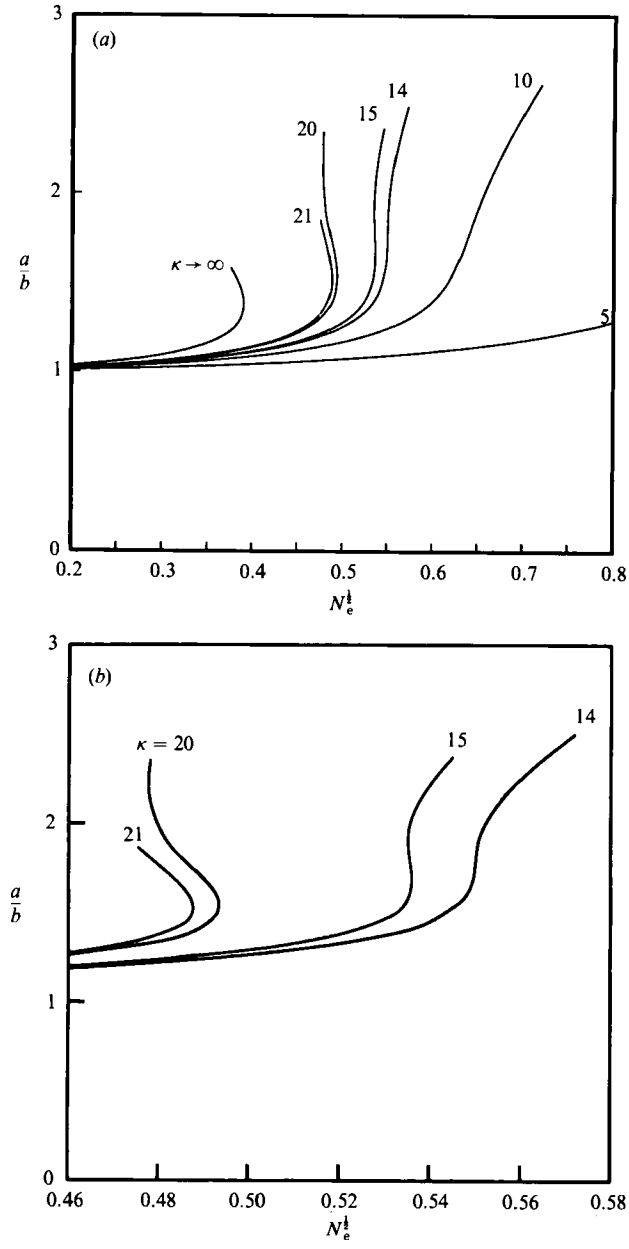

FIGURE 9. (*a*) Variation of aspect ratio a/b of initially hemispherical drops whose contact lines are fixed with field strength for various values of κ. (*b*) Blow-up of the region showing transition in types of response.

drop deformation exhibits hysteresis. With increasing aspect ratio, there is a loss of stability at the first turning point, which is subsequently regained at the second turning point. Beyond the second turning point, the drop deformation increases with increasing field strength over the region of field strengths examined. Therefore, fixing the contact line of a drop instead of prescribing its contact angle enlarges the window of values of κ for which hysteresis can be observed. (iii) When $\kappa > 20.5 \pm 0.5$, families of equilibrium drop shapes lose stability at turning points with respect to field

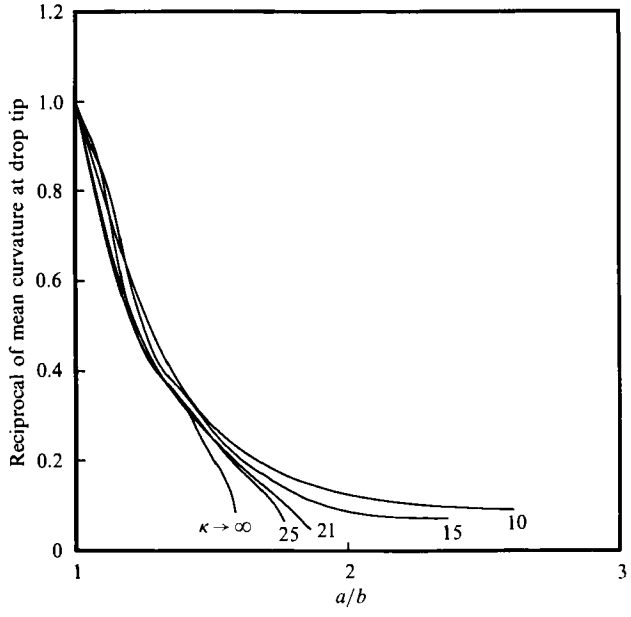

FIGURE 10. Variation of the reciprocal of the average mean curvature at the drop tip with increasing aspect ratio for initially hemispherical drops whose contact lines are fixed.

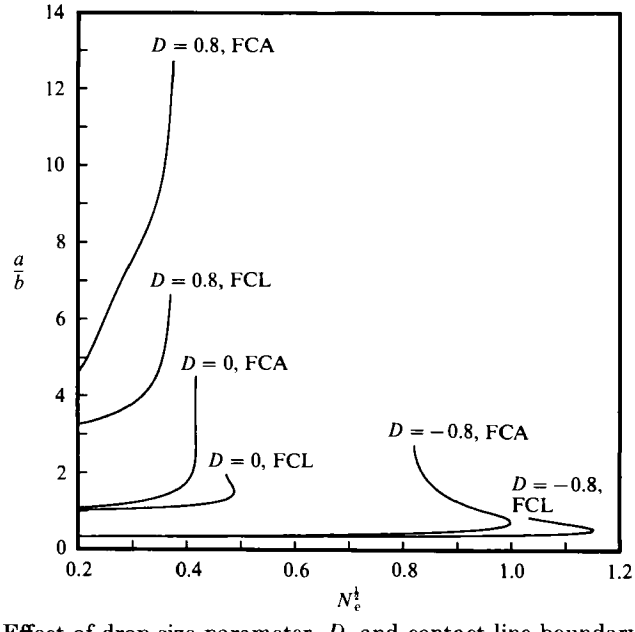

FIGURE 11. Effect of drop size parameter, D, and contact-line boundary condition on drop stability for situations in which $\kappa = 21$: FCL, fixed contact line; FCA, fixed contact angle.

strength. These families terminate beyond the turning points. This is the first time that the shapes and stability of dielectric drops whose contact lines are fixed have been calculated.

Figure 10 shows the variation of the reciprocal of the average mean curvature at the drop tip with increasing aspect ratio for initially hemispherical ($D = 0$) drops

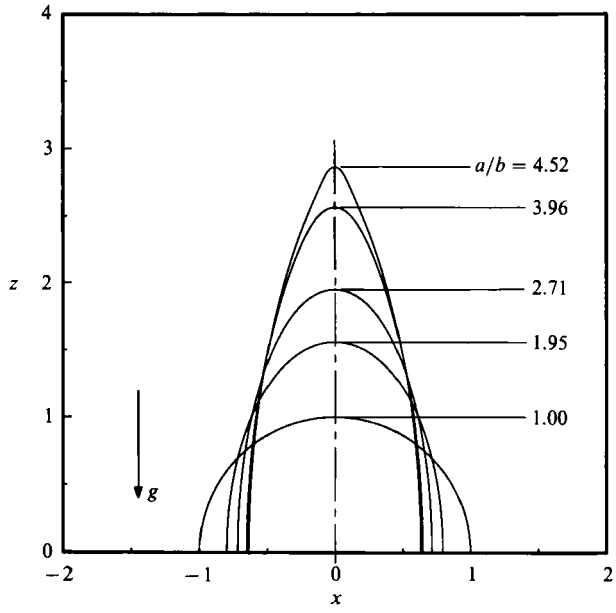

FIGURE 12. Drop shapes of axisymmetric supported drops when $G = 0$, $D = 0$, $H = S_* = 20$, and $\kappa = 21$; fixed contact angle. Values of the parallel-plate electric field strength corresponding to the aspect ratios shown are 0 for $a/b = 1.00$, 0.4088 for $a/b = 1.95$, 0.4172 for $a/b = 2.71$, 0.4163 for $a/b = 3.96$, and 0.4172 for $a/b = 4.52$.

whose contact lines are fixed. When $\kappa > 20.5 \pm 0.5$, the mean curvature at the drop tip initially increases smoothly, then rapidly goes to infinity. When $\kappa < 20.5 \pm 0.5$, the mean curvature decreases smoothly over the entire range of aspect ratios studied and evidently tends to infinity only asymptotically.

Figure 11 shows the effect of drop size parameter, D, and contact-line boundary condition on drop stability for situations in which $\kappa = 21$. As expected, a drop whose contact line is fixed is more stable than one whose contact angle is prescribed. Also, figure 11 shows that it takes a larger field to make unstable a small drop than one of larger volume: this has ramifications in areas such as enhanced separation processes (Byers & Perona 1988). Moreover, figure 11 shows that the drop size parameter, D, can have a profound effect on the stability/instability of supported dielectric drops in an electric field. When $D = 0.8$, regardless of whether the contact line is fixed or the contact angle is prescribed, the families lose stability at a turning point and terminate almost immediately afterwards. This latter result stands in contrast to situations where $D = 0$ and -0.8.

Figures 12–17 show sequences of drop shapes of a drop having a permittivity 21 times that of the surroundings ($\kappa = 21$). In figures 12–14 the contact angle is prescribed; in figures 15–17 the contact line is fixed. Figure 12 shows the response of an initially hemispherical drop. The first two shapes lie along the lower, stable branch of the family of equilibrium shapes shown in figure 6. The third shape is the neutrally stable, equilibrium drop shape at the first turning point. The fourth shape is the neutrally stable, equilibrium drop shape at the second turning point. The fifth shape is located on the upper stable branch of the family of equilibrium shapes. Plainly, the drop tip is becoming increasingly more conical as the aspect ratio increases, which implies that the curvature at the drop tip is tending to infinity (cf. figure 7). Figure 13 shows sequences of shapes of a drop having a drop size parameter of $D = 0.8$, i.e.

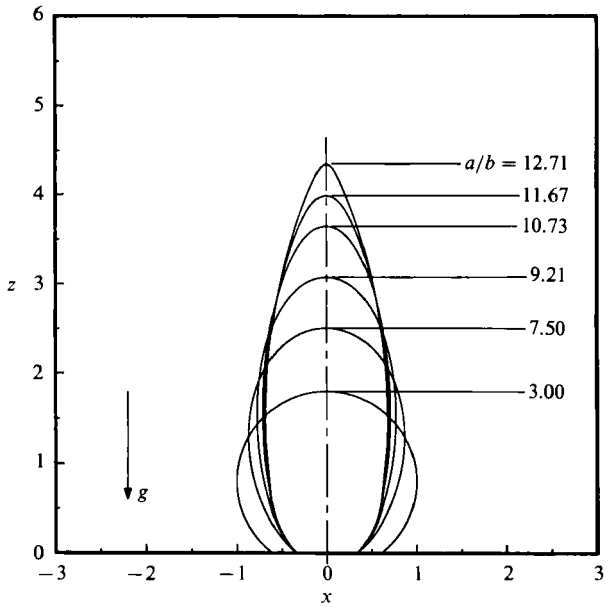

FIGURE 13. Drop shapes of axisymmetric supported drops when $G = 0$, $D = 0.8$, $H = S_* = 20$, and $\kappa = 21$; fixed contact angle. Values of the parallel-plate electric field strength corresponding to the aspect ratios shown are 0 for $a/b = 3.00$, 0.2975 for $a/b = 7.50$, 0.3478 for $a/b = 9.21$, 0.3632 for $a/b = 10.73$, 0.3711 for $a/b = 11.67$, and 0.3753 for $a/b = 12.71$.

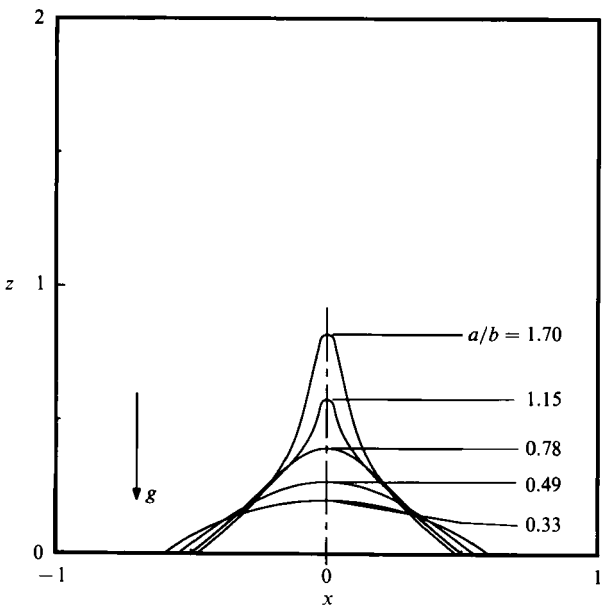

FIGURE 14. Drop shapes of axisymmetric supported drops when $G = 0$, $D = -0.8$, $H = S_* = 20$, and $\kappa = 21$; fixed contact angle. Values of the parallel-plate electric field strength corresponding to the aspect ratios shown are 0 for $a/b = 0.33$, 0.8896 for $a/b = 0.49$, 0.9976 for $a/b = 0.78$, 0.9228 for $a/b = 1.15$, and 0.8530 for $a/b = 1.70$.

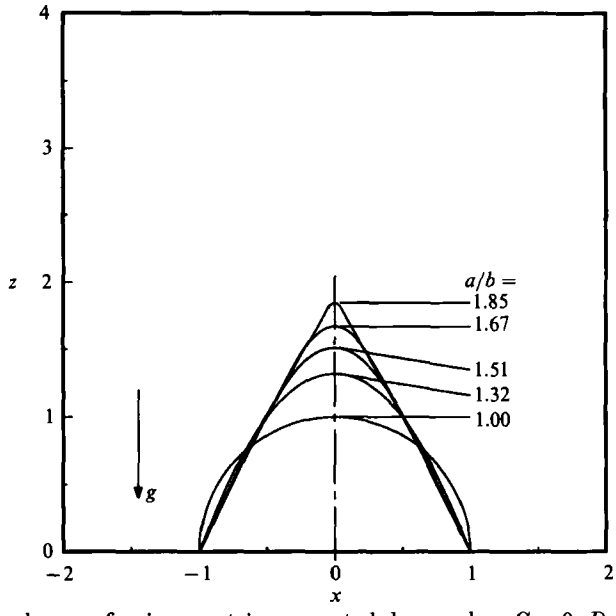

FIGURE 15. Drop shapes of axisymmetric supported drops when $G = 0$, $D = 0$, $H = S_* = 20$, and $\kappa = 21$; fixed contact line. Values of the parallel-plate electric strength corresponding to the aspect ratios shown are 0 for $a/b = 1.00$, 0.04744 for $a/b = 1.32$, 0.4880 for $a/b = 1.51$, 0.4838 for $a/b = 1.67$, and 0.4753 for $a/b = 1.85$.

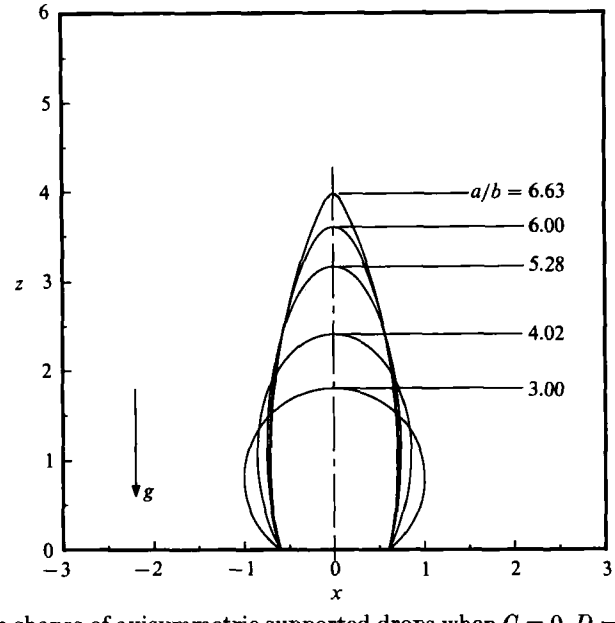

FIGURE 16. Drop shapes of axisymmetric supported drops when $G = 0$, $D = 0.8$, $H = S_* = 20$, and $\kappa = 21$; fixed contact line. Values of the parallel-plate electric field strength corresponding to the aspect ratios shown are 0 for $a/b = 3.00$, 0.3200 for $a/b = 4.02$, 0.3602 for $a/b = 5.28$, 0.3670 for $a/b = 6.00$, and 0.3708 for $a/b = 6.63$.

a drop making a fixed contact angle of about 37° with the supporting plate. All of the shapes shown in figure 13 are stable. Figure 14 shows a small drop having drop size parameter of $D = -0.8$, i.e. a drop making a fixed contact angle of about 143° with the supporting plate. The results show that drops up to an aspect ratio of 0.78 (the first three shapes shown) are stable (cf. figure 11). The unstable shapes shown of drops that lie beyond the stability limit are akin to that of a jet emanating from a liquid pool. Figure 15 shows that an initially hemispherical drop whose contact line is fixed becomes very conical as its aspect ratio increases. The first three shapes shown are stable, the last two are unstable. The large drop in figure 16 with a drop size parameter of $D = 0.8$ behaves much like the equally sized drop in figure 13 whose contact angle is prescribed. All the shapes shown in figure 16 are stable, except the last one with $a/b = 6.63$, which is the neutrally stable, equilibrium shape at the turning point. The family of shapes shown in figure 16 terminates shortly after the turning point (cf. figure 11). Figure 17 is also similar to the case of the equally sized drop with a prescribed contact angle shown in figure 14. The first three shapes are stable. The last shape is unstable and is located at the point along the branch in figure 11 where this family terminates. Again, the shape looks analogous to a jet emanating from a liquid pool, but is not as pronounced as that of the drop shown in figure 14. Drops having the same volume as but different values of κ from those shown in figures 12–17 evolve through remarkably similar profiles as they deform.

Figure 18 shows the evolution with increasing aspect ratio of the electric field vectors and equipotential lines of an initially hemispherical drop whose contact angle is fixed and which has a permittivity 21 times that of the surrounding fluid, i.e. $\kappa = 21$. The electric field vectors are scaled differently inside and outside the drop to better illustrate the relative magnitudes of the vectors in each of these regions. The electric field is virtually uniform far from the drop both near the top plate and the asymptotic side boundary. Near the drop, the electric field is seen to have a large strength and to vary rapidly compared to that far from the drop. Lines of constant potential are also highly curved in the vicinity of the drop. As the drop becomes increasingly elongated, figure 18 shows that the electric field strength builds at the drop tip. Indeed, the field strength at the drop tip can build so quickly that the electrical pressure that it generates there can no longer be counterbalanced by the action of surface tension in as highly curved a surface as the drop can develop. Figures 6, 9, and 11 show that the consequences of field concentration at the drop tips are loss of stability at turning points and ending of families of equilibrium shapes. Were the drops shown in figure 18 truly spheroids, the electric field inside them would be uniform, as is well known from classical electromagnetic theory (Landau & Lifshitz 1960). Remarkably, the field inside these drops is also nearly uniform even at very high deformations, although the shapes of such highly deformed drops are far from spheroids. The latter fact may explain in part why the spheroidal approximation has often proved useful, with the few notable exceptions detailed earlier in this paper.

Figure 19 shows the effect of plate spacing on the stability of initially hemispherical drops ($D = 0$) whose contact angles are prescribed. For $\kappa = 20$, figure 19(a) shows that when the plate spacing is changed from $H = 20$ to 10, with $S_* = H$, the computed field strength at an aspect ratio of 2.5 changes by less than 0.2%. Moreover, for a plate spacing of $H = 10$, changing the location of the asymptotic boundary S_{asym} from $S_* = 10$ to 20 changes the computed field strength at an aspect ratio of 2.5 by less than 0.1%. The latter result is not shown in figure 19(a), but establishes the insensitivity of the computed results when $H = 10$ to further changes

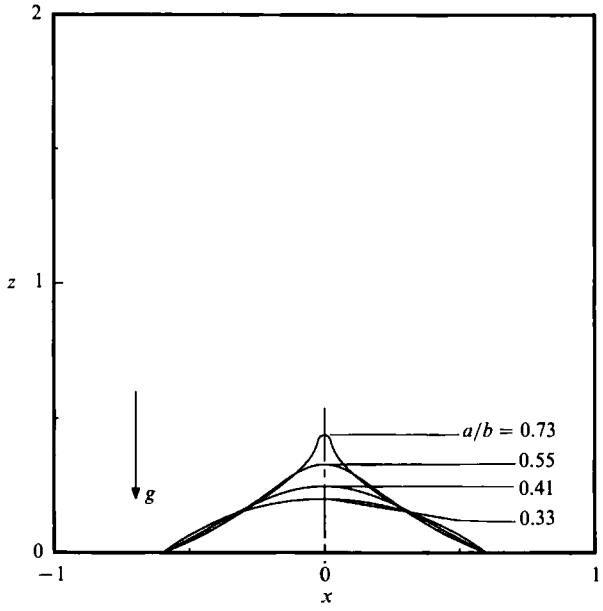

FIGURE 17. Drop shapes of axisymmetric supported drops when $G = 0$, $D = -0.8$, $H = S_* = 20$, and $\kappa = 21$; fixed contact line. Values of the parallel-plate electric field strength corresponding to the aspect ratios shown are 0 for $a/b = 0.33$, 1.0469 for $a/b = 0.41$, 1.1531 for $a/b = 0.55$, and 1.0833 for $a/b = 0.73$.

in the location of the asymptotic boundary S_{asym} so long as $S_* \geqslant H$. When the plate spacing is decreased to $H = 5$, $S_* \geqslant 10$ for computed results to be unaffected by the location of the asymptotic boundary S_{asym}. Figure 19(*a*) also shows that when $H = 5$ (with $S_* = 10$) the computed value of the field strength at an aspect ratio of 2.5 differs by about 1.2% from that when $H = 10$. However, whereas the nature of the family of equilibrium shapes in the space of aspect ratio versus field strength is monotonic when $H \geqslant 10$, it is multivalued when $H = 5$. Plainly, a drop whose aspect ratio increases monotonically with field strength when the distance between the two plates is large enough or infinite can exhibit hysteresis in drop deformation when the plates are sufficiently close. On the other hand, figure 19(*b*) shows that a drop with a higher value of κ than that of figure 19(*a*) and which exhibits hysteresis in drop deformation when the plates are sufficiently far apart will not do so when the plates are brought sufficiently close to one another. Figure 19(*b*) shows that when $\kappa = 21.5$ the family of equilibrium drop shapes exhibits hysteresis in drop deformation for $H = 20$, but terminates after the first turning point when the plate spacing is decreased to $H = 5$. When the value of κ is sufficiently different from those for which hysteresis can be observed, figures 19(*c*) and 19(*d*) show that large changes in plate spacing result in small quantitative, but not qualitative, changes in the response of the drops. At an aspect ratio of 2.5, changing the plate spacing from $H = 20$ to 5 changes the computed value of the field strength by 1.5% when $\kappa \to \infty$ and by 1.1% when $\kappa = 15$, but leaves unaffected the qualitative response of these shape families over the entire range of parameters examined.

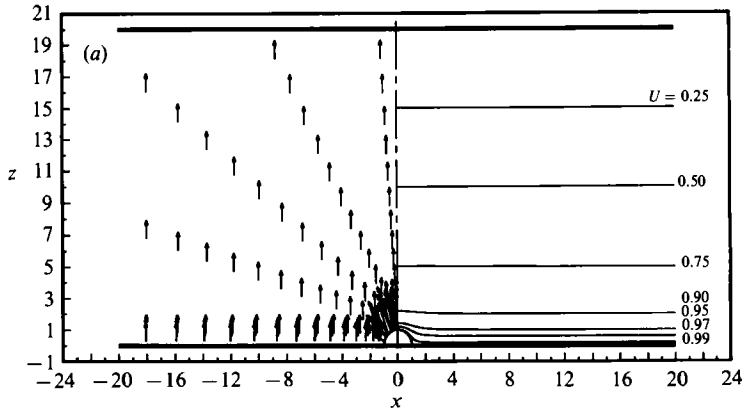

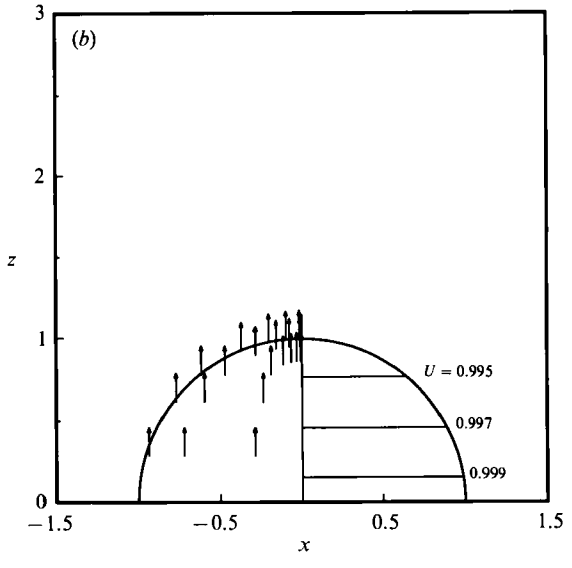

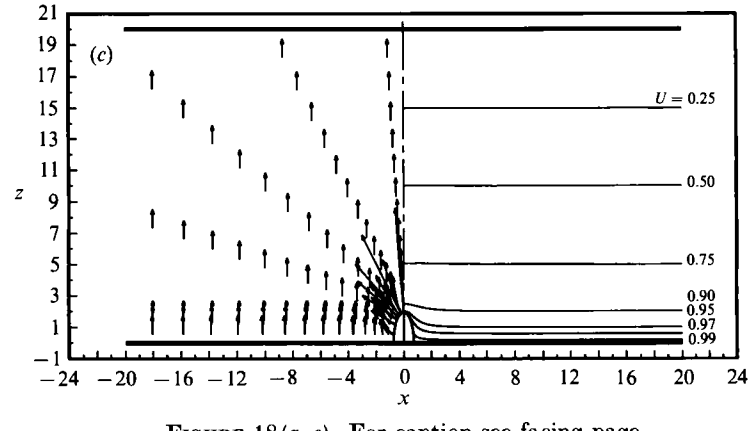

FIGURE 18(*a–c*). For caption see facing page.

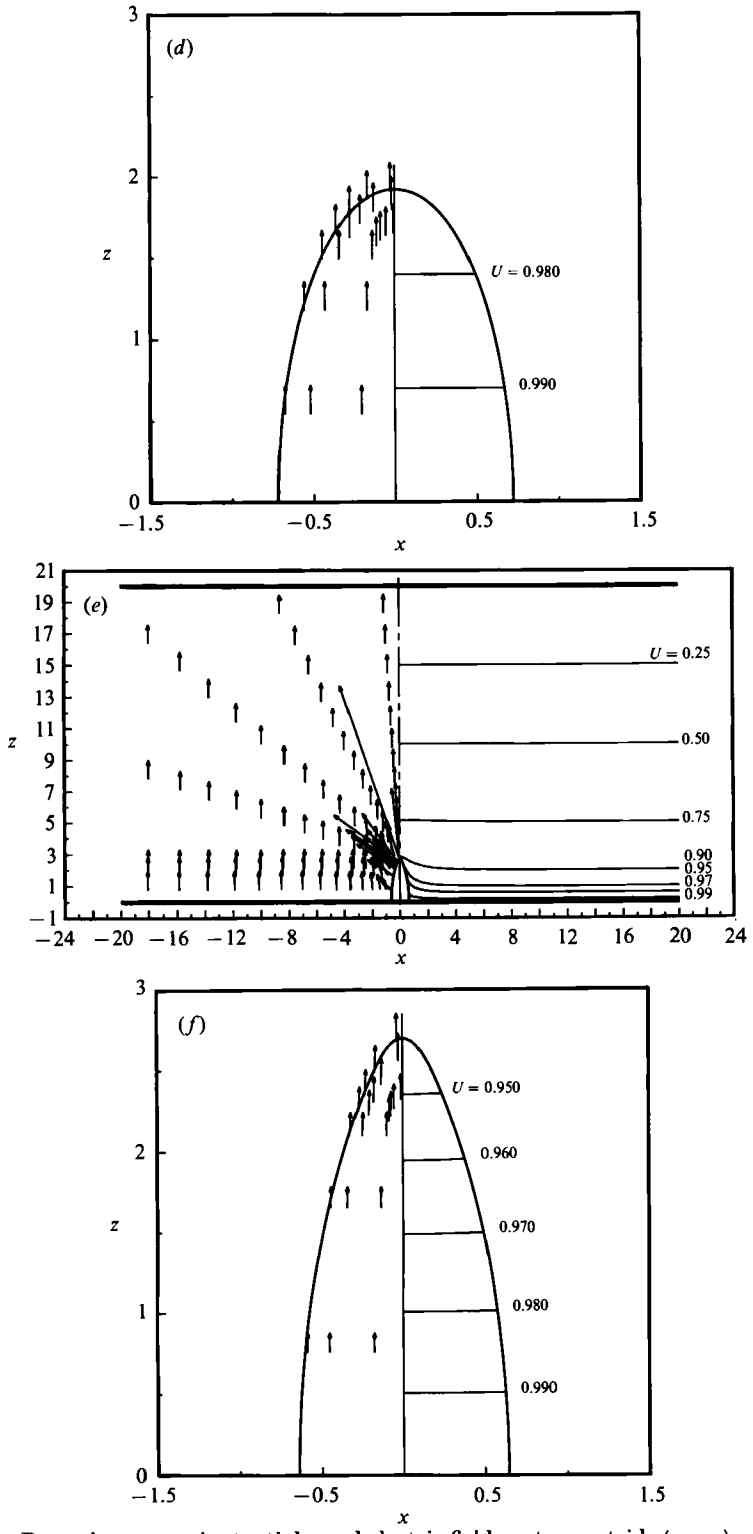

FIGURE 18. Drop shapes, equipotentials, and electric field vectors outside (a, c, e) and inside (b, d, f) a drop whose contact angle is fixed when $G = 0$, $D = 0$, $H = S_* = 20$, and $\kappa = 21$. (a), (b) $N_e^{\frac{1}{3}} \to 0$; (c), (d) $N_e^{\frac{1}{3}} = 0.4172$; (e), (f) $N_e^{\frac{1}{3}} = 0.4165$. Each field vector shown belongs to its base point.

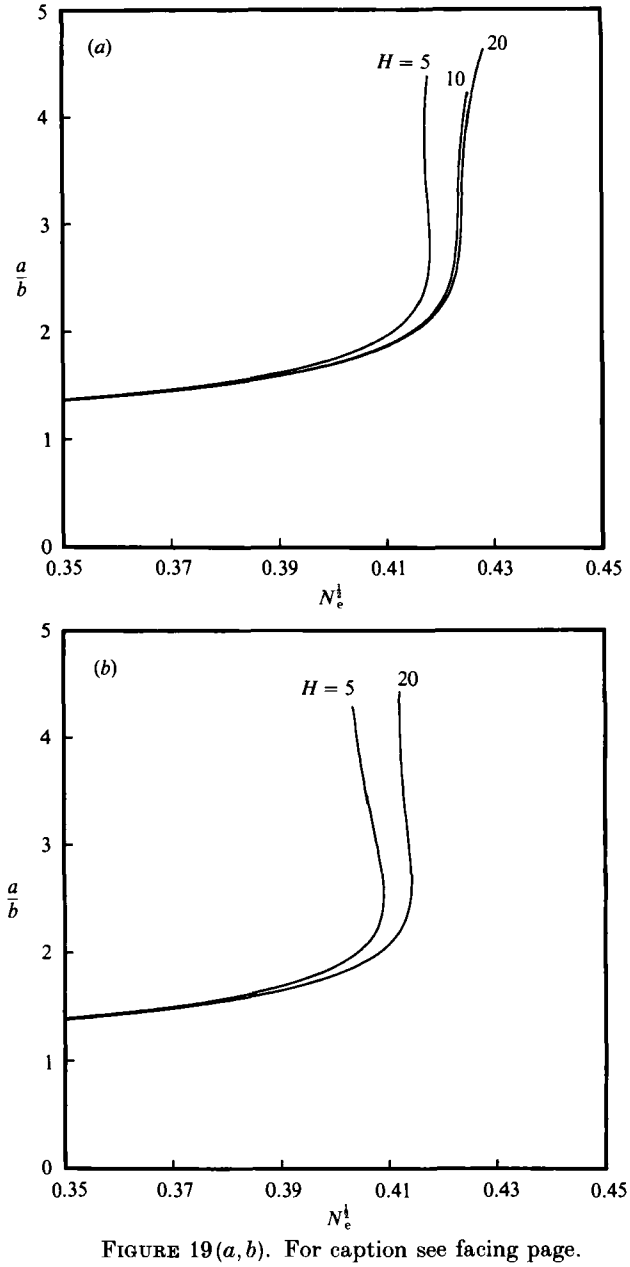

FIGURE 19(a, b). For caption see facing page.

5. Conclusions

In this paper, use of a mesh of composite cylindrical/spherical coordinates that moves as the drop deforms has allowed accurate calculation of drop shapes of very high aspect ratio. The new results conclusively show for the first time the evolution with electric field strength of families of dielectric drops and identify regions of parameter space over which hysteresis ought to be observed. Moreover, according to the foregoing results, the region of parameter space over which hysteresis can be observed is narrow, which may explain in part difficulties encountered by others in previous attempts at calculating it.

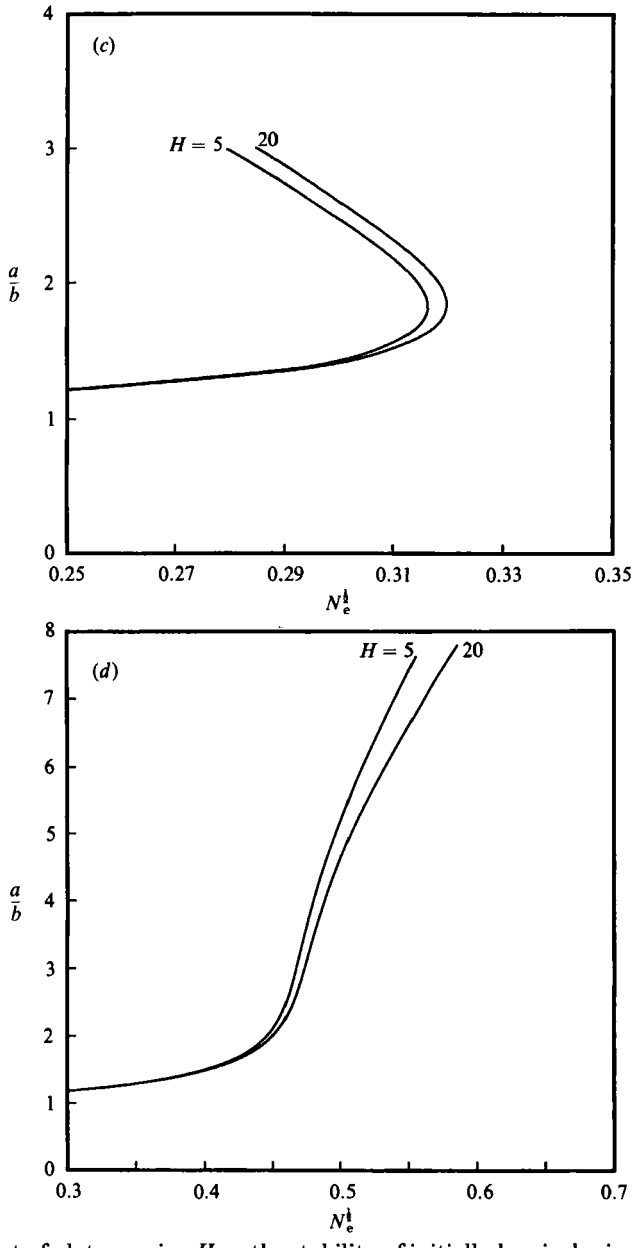

FIGURE 19. Effect of plate spacing H on the stability of initially hemispherical drops ($D = 0$) whose contact angles are prescribed: (*a*) $\kappa = 20$, (*b*) $\kappa = 21.5$, (*c*) $\kappa \to \infty$, (*d*) $\kappa = 15$.

The results of this paper show that hysteresis should be observed over the range $20.25 \pm 0.25 \leqslant \kappa \leqslant 21.75 \pm 0.25$ in situations in which (*a*) a sessile drop is hemispherical in the absence of electric field and makes a fixed contact angle of 90° with the supporting plate of a parallel-plate capacitor whose plates are infinitely far apart, and (*b*) a free drop is immersed in an externally applied field which is uniform infinitely far from the drop. In the closest experimental simulation of this situation, Bacri & Salin (1982) observed hysteresis in deformation of drops of a ferrofluid at an *apparent* value of the ratio of the drop permeability to that of the surrounding fluid

of about 40. Aside from the inherent loss in accuracy that would result from their method of determining κ (see §1), their experiments were performed with a suspension of ferrofluid drops instead of isolated drops. For a suspension of spherical drops, the effective permittivity/permeability of the suspension, ϵ_{eff}, would be related to the permittivity/permeability of the suspending fluid or the solvent, ϵ_{out}, by (Maxwell 1873; Jeffreys 1973)

$$\frac{\epsilon_{\text{eff}}}{\epsilon_{\text{out}}} = 1 + 3\left(\frac{\alpha-1}{\alpha+2}\right)\phi + f(\alpha)\,\phi^2 + \ldots . \tag{33}$$

Here ϕ is the volume fraction of drops in the suspension, $\alpha \equiv \epsilon_{\text{in}}/\epsilon_{\text{out}}$, where ϵ_{in} is the permittivity/permeability of the drops, and $f(\alpha)$ is a tabulated function (Jeffreys 1973). If $\alpha \gg 1$, then $(\alpha-1)/(\alpha+2) \approx 1$ and

$$\frac{\epsilon_{\text{eff}}}{\epsilon_{\text{out}}} = 1 + 3\phi + \ldots . \tag{34}$$

It then follows that

$$\left(\frac{\epsilon_{\text{in}}}{\epsilon_{\text{out}}}\right)_{\text{exp}} = \left(\frac{\epsilon_{\text{in}}}{\epsilon_{\text{eff}}}\right)_{\text{th}} \frac{\epsilon_{\text{eff}}}{\epsilon_{\text{out}}} . \tag{35}$$

In (35), $(\epsilon_{\text{in}}/\epsilon_{\text{out}})_{\text{exp}}$ is the actual ratio of the permittivity/permeability of the drop to that of the surrounding fluid in the experiments and $(\epsilon_{\text{in}}/\epsilon_{\text{eff}})_{\text{th}}$ is the value of κ used in theoretical calculations with a single drop. A modest loading of 10–20% would increase the *apparent* value of κ used in Bacri & Salin's (1982) experiments by roughly 50% over that used in the theoretical calculations.

In a typical ferrofluid, the relation between the applied field strength and the polarization is well-known to be nonlinear (Rosensweig 1985). The theoretical analysis presented in this paper and those of Miksis (1981), Sherwood (1988) and others do not account for the nonlinear polarization of the drop material in the applied field. This simplification reduces the Maxwell equations that govern the distribution of electric/magnetic field inside the drop to the Laplace equation (2) and may also account in part for the discrepancy between theoretical predictions and experimental measurements. To date, only Boudouvis *et al.* (1988) have analysed the response of polarizable drops having a nonlinear constitutive relationship between the applied field and the induced polarization. However, Boudouvis *et al.* (1988) were primarily interested in the effect of magnetic fields on the wetting behaviour of ferrofluid drops and did not carry their calculations past the turning points uncovered in this paper. Because the Maxwell equations governing the distribution of electric/magnetic field for nonlinear materials are nonlinear partial differential equations, they cannot be solved by boundary-integral methods. However, these equations are readily amenable to solution by the Galerkin/finite-element outlined in §3. Extending the present analysis to the case of nonlinearly polarizable drops is a future goal of this research.

This research was sponsored by the Division of Chemical Sciences, Office of Basic Energy Sciences (BES), US Department of Energy (DOE) under contract DE-AC05-84OR21400 with Martin Marietta Energy Systems, Inc. Calculations were carried out at the Florida State University (FSU) Computing Center under a grant from the BES Office of the US DOE. The authors would like to thank the staff of the FSU Computing Center for their support and eagerness to help. D. L. Cooper, J. E.

Rexrode, and S. A. Kaye, participants in the Oak Ridge Science and Engineering Research Semester (ORSERS) program helped in the preparation of the figures for this article.

REFERENCES

ABBOTT, J. P. 1978 An efficient algorithm for the determination of certain bifurcation points. *J. Comput. Appl. Maths* **4**, 19.

ADORNATO, P. M. & BROWN, R. A. 1983 Shape and stability of levitated drops. *Proc. R. Soc. Lond.* A **389**, 101.

BACRI, J. C. & SALIN, D. 1982 Instability of ferrofluid magnetic drops under magnetic field. *J. Phys. Lett.* **43**, L649.

BACRI, J. C. & SALIN, D. 1983 Dynamics of the shape transition of a ferrofluid magnetic drop. *J. Phys. Lett.* **44**, L415.

BACRI, J. C., SALIN, D. & MASSART, R. 1982 Shape of the deformation of ferrofluid droplets in a magnetic field. *J. Phys. Lett.* **43**, L179.

BASARAN, O. A., SCOTT, T. C. & BYERS, C. H. 1989 Drop oscillations in liquid–liquid systems. *AIChE J.* **35**, 1263.

BASARAN, O. A. & SCRIVEN, L. E. 1982 Profiles of electrified drops and bubbles. In *Proc. Second Intl Colloq. on Drops and Bubbles* (ed. D. H. LeCroissette). Jet Propulsion Laboratory, Pasadena, CA.

BASARAN, O. A. & SCRIVEN, L. E. 1989*a* Axisymmetric shapes and stability of isolated charged drops. *Phys. Fluids* A **1**, 795.

BASARAN, O. A. & SCRIVEN, L. E. 1989*b* Axisymmetric shapes and stability of charged drops in an external electric field. *Phys. Fluids* A **1**, 799.

BASARAN, O. A. & SCRIVEN, L. E. 1990 Axisymmetric shapes and stability of pendant and sessile drops in an electric field. *J. Colloid Interface Sci.* **140**, 10.

BEARD, K. V., OCHS, H. T. & KUBESH, R. J. 1989 Natural oscillations of small raindrops. *Nature* **342**, 408.

BENNER, R. E., BASARAN, O. A. & SCRIVEN, L. E. 1991 Equilibria, stability and bifurcations of rotating columns of fluid subjected to planar disturbances. *Proc. R. Soc. Lond.* A **433**, 81.

BERKOVSKY, B. M., BASHTOVOI, V., MIKHALEV, V. & REX, A. 1987 Experimental study of the stability of bounded volumes of magnetic fluid with a free surface. *J. Magnetism Magn. Mater.* **65**, 239.

BERKOVSKY, B. M. & KALIKMANOV, V. I. 1985 Topological instability of magnetic fluids. *J. Phys. Lett.* **46**, L483.

BOHR, N. & WHEELER, J. A. 1939 The mechanism of fission. *Phys. Rev.* **56**, 426.

BOUDOUVIS, A. G., PUCHALLA, J. L. & SCRIVEN, L. E. 1988 Magnetohydrostatic equilibria of ferrofluid drops in external magnetic fields. *Chem. Engng Commun.* **67**, 129.

BRANCHER, J. P. & ZOUAOUI, D. 1987 Equilibrium of a magnetic liquid drop. *J. Magnetism Magn. Mater.* **65**, 311.

BRAZIER-SMITH, P. R. 1971 Stability and shape of isolated and pairs of water drops in an electric field. *Phys. Fluids* **14**, 1.

BUDNIK, A. M. & POLEVIKOV, V. K. 1987 Numerical study of equilibrium forms of magnetic fluid including magnetic field disturbances. *J. Magnetism Magn. Mater.* **65**, 335.

BYERS, C. H. & PERONA, J. J. 1988 Drop formation from an orifice in an electric field. *AIChE J.* **34**, 1577.

CARRUTHERS, J. R. & TESTARDI, L. R. 1983 Materials processing in the reduced-gravity of space. *Ann. Rev. Mater. Sci.* **13**, 247.

CHANDRASEKHAR, S. 1969 *Ellipsoidal Figures of Equilibrium.* Yale University Press.

CHANG, L. S. & BERG, J. C. 1985 The effect of interfacial tension gradients on the flow structure of single drops or bubbles translating in an electric field. *AIChE J.* **31**, 551.

COHEN, S., PLASIL, R., & SWIATECKI, W. J. 1974 Equilibrium configurations of gravitating liquid masses with surface tension. *Annls Phys.* **82**, 557.

FRANKLIN, B. 1751 *New Experiments and Observations on Electricity Made at Philadelphia in America*. Printed by E. Cave at St John's Gate.

GUPTE, S. M. & TSAMOPOULOS, J. A. 1989 Densification of porous materials by chemical vapor infiltration. *J. Electrochem. Soc.* **136**, 555.

HOOD, P. 1976 Frontal solution program for unsymmetric matrices. *Intl J. Numer. Meth. Engng* **10**, 379, and Correction, *Intl J. Num. Meth. Engng* **11** (1977), 1055.

IOOSS, G. & JOSEPH, D. D. 1990 *Elementary Stability and Bifurcation Theory*. Springer.

ISAACSON, E. & KELLER, H. B. 1966 *Analysis of Numerical Methods*. John Wiley.

JEFFREYS, D. J. 1973 Conduction through a random suspension of spheres. *Proc. R. Soc. Lond.* A **355**, 355.

KISTLER, S. F. & SCRIVEN, L. E. 1983 Coating flows. In *Computational Analysis of Polymer Processing* (ed. J. R. A. Pearson & S. M. Richardson). Applied Science Publishers.

LANDAU, L. D. & LIFSHITZ, E. M. 1960 *Electrodynamics of Continuous Media*. Pergamon.

MAXWELL, J. C. 1873 *Electricity and Magnetism*. Clarendon.

MELCHER, J. R. 1981 *Continuum Electromechanics*. MIT Press.

MELCHER, J. R. & TAYLOR, G. I. 1969 Electrohydrodynamics: a review of the role of interfacial shear stresses. *Ann. Rev. Fluid Mech.* **1**, 111.

MIKSIS, M. J., 1981 Shape of a drop in an electric field. *Phys. Fluids* **24**, 1967.

ORTEGA, J. M. & RHEINBOLDT, W. C. 1970 *Iterative Solution of Nonlinear Equations in Several Variables*. Academic.

PELEKASIS, N. A., TSAMOPOULOS, J. A. & MANOLIS, G. D. 1990 Equilibrium shapes and stability of charged and conducting drops. *Phys. Fluids* A **2**, 1328.

RAYLEIGH, LORD 1879 The influence of electricity on colliding water drops. *Proc. R. Soc. Lond.* A **28**, 406.

RAYLEIGH, LORD 1882 On the equilibrium of liquid conducting masses charged with electricity. *Phil. Mag.* **14**, 184.

RHIM, W. K., CHUNG, S. K. & ELLEMAN, D. D. 1989 Experiments on rotating charged liquid drops. In *Proc. Third. Intl Colloquium on Drops and Bubbles* (ed. T. G. Wang). American Institute of Physics.

ROSENKILDE, C. E. 1969 A dielectric fluid drop in an electric field. *Proc. R. Soc. Lond.* A **312**, 473.

ROSENSWEIG, R. E. 1979 Fluid dynamics and science of magnetic liquids. In *Advances in Electronics and Electron Physics*, Vol. 48 (ed. L. Marton). Academic.

ROSENSWEIG, R. E. 1985 *Ferrohydrodynamics*. Cambridge University Press.

SAITO, H. & SCRIVEN, L. E. 1981 Study of coating by the finite element method. *J. Comput. Phys.* **42**, 53.

SARTOR, J. D. 1969 Electricity and rain. *Phys. Today* **22**, 45.

SHERWOOD, J. D. 1988 Breakup of fluid droplets in electric and magnetic fields. *J. Fluid Mech.* **188**, 133.

STRANG, G. & FIX, G. J. 1973 *An Analysis of the Finite Element Method*. Prentice-Hall.

TAYLOR, G. I. 1964 Disintegration of water drops in an electric field. *Proc. R. Soc. Lond.* A **280**, 383.

UNGAR, L. H. & BROWN, R. A. 1982 The dependence of the shape and stability of captive rotating drops on multiple parameters. *Phil. Trans. R. Soc. Lond.* A **306**, 347.

UNGAR, L. H. & BROWN, R. A. 1985 Cellular interface morphologies in directional solidification IV. The formation of deep cells. *Phys. Rev.* B **31**, 5931.

WALTERS, R. A. 1980 The frontal method in hydrodynamics simulations. *Comput. Fluids* **8**, 265.

WEATHERBURN, C. E. 1927 *Differential Geometry of Three Dimensions*. Cambridge University Press.

WILSON, C. T. R. & TAYLOR, G. I. 1925 The bursting of soap-bubbles in a uniform electric field. *Proc. Camb. Phil. Soc.* **22**, 98.